UNIVERSITY OF HELSINKI REPORT SERIES IN PHYSICS

HU-P-D168

Computer simulation of H and He effects in fusion reactor materials

Niklas Juslin

Division of Materials Physics
Department of Physics
Faculty of Science
University of Helsinki
Helsinki, Finland

ACADEMIC DISSERTATION

To be presented, with the permission of the Faculty of Science of the University of Helsinki, for public criticism in the Small Auditorium E204 of the Department of Physics (Physicum), on October 31st 2009, at 10 o'clock a.m.

HELSINKI 2009

ISBN 978-952-10-5640-6 (printed version)
ISSN 0356-0961
Helsinki 2009
Helsinki University Printing House (Yliopistopaino)

ISBN 978-952-10-5641-3 (PDF version)
http://ethesis.helsinki.fi/
Helsinki 2009
Electronic Publications @ University of Helsinki (Helsingin yliopiston verkkojulkaisut)

Niklas Juslin **Computer simulation of H and He effects in fusion reactor materials**, University of Helsinki, 2009, 49 p.+appendices, University of Helsinki Report Series in Physics, HU-P-D168, ISSN 0356-0961, ISBN 978-952-10-5640-6 (printed version), ISBN 978-952-10-5641-3 (PDF version)

Classification (INSPEC): A2852F, A3420, A6180, A711M
Keywords (INSPEC): iron,chromium,helium,tungsten,hydrogen,carbon,reactor materials,fusion reactors,damage,cascades,irradiation,potential development,molecular dynamics,density functional theory

ABSTRACT

Fusion power is an appealing source of clean and abundant energy. The radiation resistance of reactor materials is one of the greatest obstacles on the path towards commercial fusion power. These materials are subject to a harsh radiation environment, and cannot fail mechanically or contaminate the fusion plasma. Moreover, for a power plant to be economically viable, the reactor materials must withstand long operation times, with little maintenance.

The fusion reactor materials will contain hydrogen and helium, due to deposition from the plasma and nuclear reactions because of energetic neutron irradiation. The first wall divertor materials, carbon and tungsten in existing and planned test reactors, will be subject to intense bombardment of low energy deuterium and helium, which erodes and modifies the surface. All reactor materials, including the structural steel, will suffer irradiation of high energy neutrons, causing displacement cascade damage.

Molecular dynamics simulation is a valuable tool for studying irradiation phenomena, such as surface bombardment and the onset of primary damage due to displacement cascades. The governing mechanisms are on the atomic level, and hence not easily studied experimentally. In order to model materials, interatomic potentials are needed to describe the interaction between the atoms.

In this thesis, new interatomic potentials were developed for the tungsten-carbon-hydrogen system and for iron-helium and chromium-helium. Thus, the study of previously inaccessible systems was made possible, in particular the effect of H and He on radiation damage. The potentials were based on experimental and *ab initio* data from the literature, as well as density-functional theory calculations performed in this work.

As a model for ferritic steel, iron-chromium with 10% Cr was studied. The difference between Fe and FeCr was shown to be negligible for threshold displacement energies. The properties of small He and He–vacancy clusters in Fe and FeCr were also investigated. The clusters were found to be more mobile and dissociate more rapidly than previously assumed, and the effect of Cr was small.

The primary damage formed by displacement cascades was found to be heavily influenced by the presence of He, both in FeCr and W.

Many important issues with fusion reactor materials remain poorly understood, and will require a huge effort by the international community. The development of potential models for new materials and the simulations performed in this thesis reveal many interesting features, but also serve as a platform for further studies.

Contents

1 INTRODUCTION

Fusion power is an enticing solution to the energy production problems faced presently and in the future. While the fusion process is well understood, fusion power production has, however, remained elusive. Test reactors capable of producing almost as much energy as put in exist, but one of the major problems in achieving commercial fusion power is developing materials able to withstand the extreme environment in a reactor. There is particular interest in two types of materials, the structural steel needed for the construction of the reactor, and the first wall material which is subject to the heaviest heat load of ions from the plasma.

The study of radiation damage in materials is a vast field, with irradiating species ranging in size from electrons up to large molecules and clusters, and in energy from eV to GeV. The irradiated materials can be, among many others, nuclear reactor and accelerator walls, satellites or biological materials. In this thesis the focus is on radiation damage in fusion reactor walls. While irradiation can have positive and desired effects, generally it deteriorates the material, by causing structural damage at the surface or in the bulk. In particular high energy particles can cause extensive damage, as well as nuclear reactions, inside a material.

The first wall of the reactor will be bombarded with deuterium and helium, mostly of relatively low energy, causing surface modification, and ejection of material from the surface. A thorough understanding of these phenomena is important in order to construct a wall capable of withstanding the irradiation and not affecting the plasma during sustained reactor operation. With current technology no material can last the full lifetime of a reactor, but shutting down the reactor to exchange the wall plates must be kept to a minimum for commercial energy production.

As energetic neutrons are produced in the fusion process, they will irradiate the whole reactor, including the first wall and the structural steel. As they hit atoms inside the materials, they will cause displacement cascades, which lead to primary damage formation, *i.e.* defects that remain after the cascades cool down. The neutrons also lead to production of helium due to nuclear reactions, and thus the reactor materials will contain helium. As helium can affect the mechanical properties and radiation resistance of the materials it is important to study the materials with a presence of helium.

As many important irradiation related phenomena take place on an atomistic level and a short time scale, and while the material is being irradiated, studying them experimentally can be problematic. Computer calculations can help improve the understanding of how the materials behave under irradiation, as well as predict which materials could be used in a reactor. Electronic structure calculations such as density-functional theory (DFT), can be used to calculate basic mechanical and defect properties, but are still too computer power intensive to be used for systems larger than a few hundred

or thousand atoms. Molecular dynamics (MD), which does not explicitly include electrons, is well suited for simulations of up to millions of atoms and times up to nanoseconds. Different Monte Carlo (MC) methods can be used for even larger systems or longer times, but in order to go up in scale, some approximations always have to be made.

There are two types of studies in this thesis. The development of potentials for modeling the interaction between atoms for MD simulations, allowing study of previously inaccessible materials. These potentials are based on experimental and *ab initio* literature data, as well as DFT calculations performed within this work. Some of these potentials, along with potentials by other groups, are used to study production of irradiation damage, in particular the effect of helium and chromium in iron chromium, and helium in tungsten.

2 PURPOSE AND STRUCTURE OF THIS STUDY

The purpose of this thesis is to develop interatomic potentials designed for molecular dynamics simulations of irradiation of fusion reactor materials, as well as to apply the potentials to study defect structures and irradiation properties.

This thesis consists of six publications, referred to by roman numerals (**I-VI**). The first five are published in peer-reviewed journals, while the last one has been submitted for review. In this section, the articles are summarized and the contributions by the author explained. In Sect. 3 an overview of the fusion reactor concept and the irradiation of wall materials is given. In Sect. 4 the methods used for the studies in this thesis are presented. The potential development work is described in Sect. 5. In Sect. 6, the study of migration and clustering of He in Fe and FeCr is discussed and in Sect. 7 the irradiation results are presented. Finally the work done in this thesis is summarized in Sect. 8.

2.1 Summaries of the original publications

In publication **I**, a potential set for the W–C–H system was developed. Electronic structure calculations were performed to extend the database for fitting and testing of the potentials. In publication **II** a potential for helium in iron was developed and in publication **III** it was complemented with a potential for helium in chromium, and the potentials are used to study migration and formation of small He–vacancy clusters in Fe and FeCr using molecular dynamics simulations. In publication **IV** the role of Cr on displacement threshold energies in FeCr was investigated. The effort to understand the pri-

mary damage formation continues in publication **V**, with the study of the effect of He on displacement cascades in FeCr, and further, the effect of He on cascades in tungsten in publication **VI**.

Publication I: Analytical interatomic potential for modeling non-equilibrium processes in the W-C-H system, N. Juslin, P. Erhart, P. Träskelin, J. Nord, K.O.E Henriksson, E. Salonen, K. Nordlund and K. Albe, *J. Appl. Phys.* **98**, 123520 (2005).

In order to be able to study the W–C–H system, bond-order potentials were created for W–W, W–C and W–H to be used together with existing potentials for C–C, C–H and H–H. The W–C–H system is of interest for studying deuterium bombardment of tungsten and tungsten carbide first wall materials in fusion reactors. The bond-order potential fitting scheme from previous work was improved to better describe body-centered cubic materials and metal carbides, by extending it to second-nearest neighbor interactions. Density-functional calculations were performed to extend the data available for fitting and testing. The mechanical, defect, surface and melting properties were tested for the new potentials.

Publication II: Pair potential for Fe-He, N. Juslin and K. Nordlund, *J. Nucl. Mater.* **382**, 143-146 (2008).

As the steel in fusion reactor walls will contain helium due to nuclear reactions from high energy neutron bombardment, it is of great interest to study the effect of helium on iron. A new potential for the Fe–He interaction was developed, intended for use with the iron potentials best suited for radiation damage studies. It was shown that a repulsive pair potential is capable of reproducing *ab initio* He interstitial properties.

Publication III: Fast 3D migration of He clusters in bcc Fe and Fe-Cr alloys, D. Terentyev, N. Juslin, K. Nordlund and N. Sandberg, *J. Appl. Phys.* **105**, 103509 (2009).

The properties of small helium-vacancy (He-V) and pure He clusters in Fe and in Fe_{90}-Cr_{10} (Fe-10Cr) random alloy was studied. The focus was on the diffusion mechanisms of He-V clusters and whether Cr influences the mobility and stability of He-V clusters in the Fe-10Cr alloy. The development of the Cr–He potential is also presented. 10% Cr does not significantly affect the migration of He and the dissociation energies of He-V clusters. Small pure He clusters were found to be more mobile than previously assumed, but their mobility is retarded by the presence of Cr.

Publication IV: Simulation of threshold displacement energies in FeCr, N. Juslin, K. Nordlund, J. Wallenius and L. Malerba, *Nucl. Instr. Meth. Phys. Res. B* **255**, 75-77 (2006).

The role of chromium on threshold displacement energies in FeCr for the fusion reactor steel relevant concentration 10% Cr was studied using molecular dynamics simulations. Threshold energies were compared for pure Fe, pure Cr and FeCr with two different potential sets for Fe–Cr. No significant differences were found between pure iron and FeCr with 10% Cr for the 100, 110 and 111 directions and the average threshold energy, while they are different for pure Cr.

Publication V: Molecular dynamics simulations of collision cascades in FeCrHe, N. Juslin and K. Nordlund, *Nucl. Instr. Meth. Phys. Res. B* **267**, 3420-3423 (2009).

The effect of He on displacement cascades in FeCr with 10% Cr was studied. The primary damage formed in the material due to 1 and 5 keV recoils was analyzed with both interstitial and substitutional He. The helium concentrations were 0.1%, 0.5% and 1%. At the lowest concentration there is no discernible effect on the number of Frenkel pairs formed, while at higher concentrations, there is a significant increase in damage for interstitial He and decrease for substitutional He. The positions of the He interstitials and clusters depend on the Cr atoms and the amount of He inside the cascade region is increased by about 30% due to the cascade.

Publication VI: Effect of He on displacement cascades in W, N. Juslin, V. Jansson and K. Nordlund, *Submitted for publication to Phil. Mag. A* (2009).

A fusion reactor divertor made of tungsten will contain helium due to implantation from the plasma and transmutation reaction. He will affect the material properties and radiation damage. Molecular dynamics simulation was used to study how the presence of He affects displacement cascades in W. Three different W–W potentials were compared and found to agree that the overall effect of He is an increase in damage for interstitial He and reduction for substitutional He. This is explained by the interaction of He with vacancies as the cascade cools down. Differences between the potentials were noted particularly in the clustering of vacancies.

2.2 Author's contribution

In publication **I** the author performed all the *ab initio* calculations and all the work on W–H, as well as parts of the development and testing of the W–W and W–C potentials. For publications **II**, **IV** and **V** the author did all the work. In publication **III** the author did the potential development, except the electronic structure calculations, as well as parts of the work on migration and clustering. In publication **VI** the simulation setup and interpretation of the results were done by the author, but most of the simulations were carried out by a student supervised by the author. The author wrote articles **II**, **IV**, **V** and **VI** in their entirety, and wrote parts of the text of articles **I** and **III**.

3 FUSION REACTOR MATERIALS

At present, fusion appears to be a realistic power source for the future. If the scientific and technological problems associated with building a commercial fusion power plant are solved, mankind will have the clean and safe energy production needed to replace fossil fuel and fission power plants. The deuterium and tritium fuel needed for the fusion process can be produced in abundance from sea water and lithium from the earth's crust. There is no risk of a run away chain reaction causing a nuclear meltdown, nor is any long term radioactive waste produced.

Fusion power has, however, remained elusive. The scientific and technological difficulties in starting and maintaining a controlled fusion reaction has kept commercial fusion power "50 years away" the whole second half of the 20th century. While many fusion reactor designs have been suggested, currently the best candidate is considered to be the tokamak type reactor. There are high hopes that the viability of commercial power will be shown within the next 20-30 years. While it today is possible to approach a positive energy balance in a reactor, much remains to be done in order to keep the fusion process sustained and the reactor materials from falling apart.

In the tokamak reactor concept, the hot plasma is contained and kept away from the walls, by strong, toroidal magnetic fields. In the fusion process, hydrogen isotopes, deuterium and deuterium or deuterium and tritium, are fused into helium, producing energetic neutrons. While the neutrons carry energy out of the plasma and are used to heat the coolant liquid that would be used to drive turbines and produce electrical power, they are also a problem, as they irradiate the walls and structural material of the reactor.

Presently, the ITER [1, 2] test reactor is being built (Fig. 1). It is planned to achieve a Q value, the ratio between energy produced and that used to heat the plasma, of 10 and to be able to sustain plasma operation for several minutes. It is a tokamak reactor, and the vacuum vessel, shown in Fig. 2 will be built from steel, with beryllium wall plates covering the surfaces. The divertor (Sect. 3.1.1) in ITER will initially be be made of carbon, and later switched to tungsten.

3.1 Irradiation of reactor materials

There will be two main types of irradiation of the materials in a fusion reactor. The leakage of ions from the plasma is directed towards the divertor region, where mainly D ($\sim$90%) and He ($\sim$10%) in the low energy range of 1-100 eV will hit the surface. High energy, 14 MeV, neutrons produced in the fusion process will penetrate deeper into the reactor walls. As they are neutral, they are not contained by the magnetic field and will irradiate all parts of the reactor.

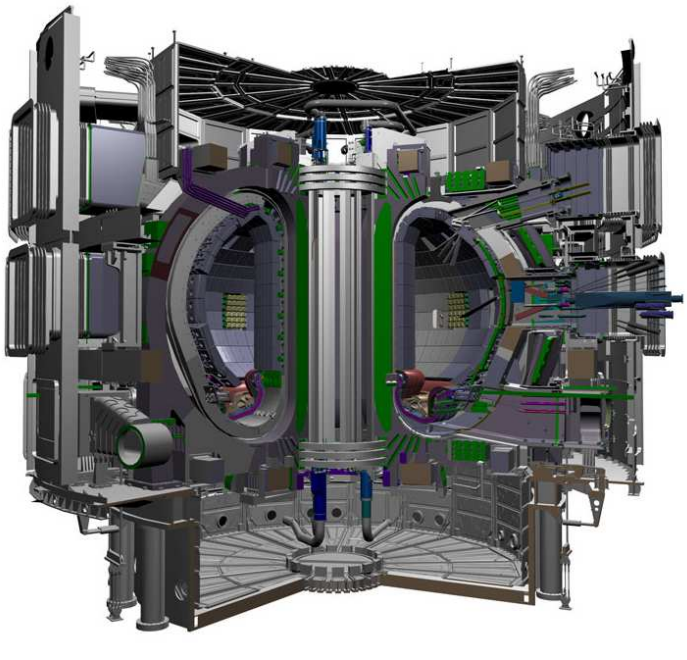

Figure 1: The ITER test reactor. In this thesis the focus is on the steel used for constructing the vacuum vessel (Fig. 2), and the divertor materials. The picture is from the ITER webpage [3] ©ITER Organization.

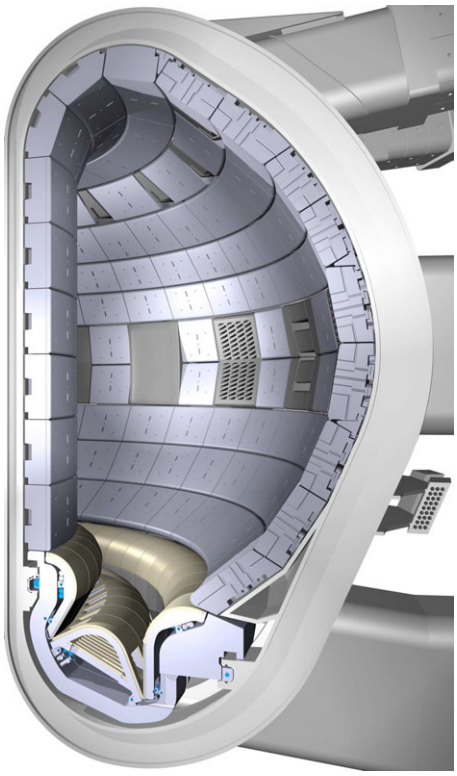

Figure 2: The vacuum vessel of the ITER test reactor. It will be constructed from steel and covered with beryllium wall plates. The bottom region, the divertor, will initially be covered with carbon plates, and later switched to tungsten. The picture is from the ITER webpage [3] ©ITER Organization.

3.1.1 The divertor

The divertor (Fig. 2) in tokamak type fusion reactors, is the bottom region of the reactor vessel. As some leakage from the plasma is unavoidable, and even desired, the magnetic fields direct it towards the divertor, which has been designed to handle the intense heat load and irradiation of 1-100 eV deuterium. Even with some of the strongest and most irradiation resistant materials available, it is expected that the divertor plates will have to be exchanged every few years of operation.

The best elemental composition of the divertor has been widely debated. The material must have excellent thermal and mechanical properties and low sputtering, *i.e.* erosion of material from the surface, especially of heavy atoms. Sputtered material can end up in the plasma, cooling it depending on the atomic number Z, as well as contaminate other parts of the reactor. For some possible materials, such as carbon, significant loss of the wall material becomes a real issue.

Carbon was long considered the best divertor material, thanks to its suitable mechanical and thermal properties. The problem with carbon, however, is that it is heavily eroded in the form of hydrocarbon molecules due to deuterium bombardment from the plasma [4–9]. This also leads to radioactive tritium being redeposited on the surfaces of the whole reactor. Tungsten also has excellent mechanical properties, and is one of the strongest divertor material candidates presently. The erosion of tungsten under reactor conditions is very low, but on the other hand any tungsten contamination of the plasma will be a problem, due to its high Z. Solutions such as using a combination of carbon, tungsten or beryllium have been considered, but the radiation resistance of divertor materials still requires a lot of study.

As both hydrogen and helium bombard the surface, as well as, are created in nuclear reactions due to high energy neutron irradiation, their interactions, mobility, clustering and effect on the materials are of interest. He and H in tungsten and tungsten carbide bulk and on surfaces have been studied extensively in the literature, both experimentally and with atomistic simulations [10–19].

3.1.2 Structural steel

A reactor cannot be constructed of wall plates alone. Steel will be needed for the construction, and will be subject to the harsh environment in the reactor. Most steels are unsuitable for a prolonged fusion reactor operation. Ferritic steels with a chromium content of around 10% are considered the best alternative [20–22]. In addition, even though the amounts are small, the reactor steel may not contain elements that under irradiation produce long lived radioactive isotopes [22]. For instance, molybdenum is usually replaced with tungsten.

The plan for the ITER reactor is to use the EUROFER steel [23, 24], which has been developed for fusion reactors. The composition of a steel capable of withstanding the decades of operation needed is, however, still a major limitation to achieving commercial fusion power in the future. Studying the irradiation of steel will continue to be one of the most important fusion related tasks in the coming decades [24], both in future experimental facilities such as ITER, DEMO [20] and IFMIF [25], and with improved modeling.

Most of the ions from the plasma will be directed towards the divertor and hit plates designed for that aspect, as discussed in Sect. 3.1.1. Thus the irradiation of the structural steel will mostly be in the form of neutrons formed in the fusion process. As they are neutral, they are not confined by the magnetic field and irradiate all parts of the reactor. These neutrons will have a relatively high energy, about 14 MeV, and can cause transmutation reactions as they hit atoms in the reactor wall materials, as well as considerable damage due to collision cascades.

The Cr concentration in irradiated ferritic steel has been shown to affect the macroscopic properties, such as the ductile to brittle transition and swelling. The reason for this behavior is not well understood [26–29] and whether the presence of Cr affects the displacement threshold energies in FeCr is studied in Sect. 7.1.

As an energetic particle hits an atom in a material, it can cause a nuclear reaction, transforming the atom into other elements or isotopes. In a fusion reactor, the most common transmutation reactions are (n,p) and (n,α) reactions, leading to formation of hydrogen and helium in the material [30]. Due to (n,α)–transmutation reactions, helium will be produced in any steel irradiated with high energy neutrons. The production rate in a fusion reactor will be about 10-15 appm/dpa, which would lead to about 0.05-0.1% He during reactor life time. Helium will deteriorate the material properties, and also affect the production of further radiation damage [31–36].

Helium is known to form bubbles in iron and steel, but the exact interactions and mechanisms of He micro-structure formation have recently been under extensive study. Helium is trapped by vacancies, interstitials and impurities [37–41]. Recently, there have been efforts to study the interaction with larger objects such as dislocation loops [42] and grain boundaries. [42]. Helium is relatively mobile and can cluster with other He and vacancies to form bubbles [38, 43–49]. Most of the studies of helium micro-structure have, however, been done with atomistic simulations or rate theory models, and thus it is important to further test and improve the modeling.

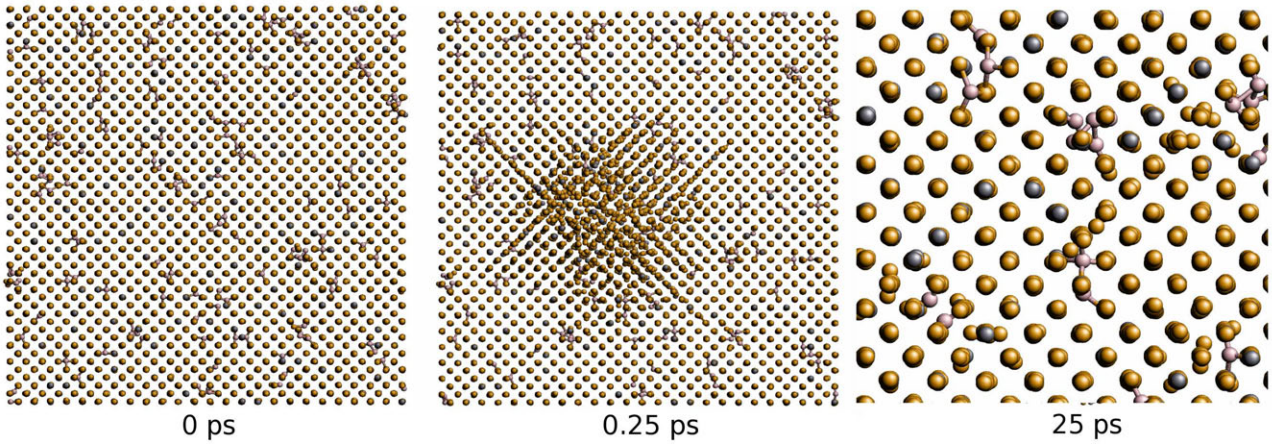

Figure 3: A typical 1 keV cascade for FeCr with 0.5% interstitial He. The color code is Fe: orange, Cr: grey and He: pink. The first frame (0 ps) is actually after a 25 ps initial equilibration, at which time a recoil energy is given. The second frame (0.25 ps) shows the peak of the heat spike, and the final frame shows a close up of the center region after 25 ps, when most of the damage has recombined, with only a few Frenkel pairs remaining as primary damage.

3.1.3 Displacement cascades and threshold energy

As a bombarding particle hits an atom in the material, the primary knock-on atom (PKA), it imparts some of its energy onto the PKA. The PKA in turn hits other atoms, producing a collision cascade. Generally enough atoms are so energetic that the collision cascade forms a molten region, called a heat spike, around the PKA. As the heat spike cools down, most of the region crystallizes again. Some of the atoms can, however, fail to recombine with a vacancy and remain as interstitials, thus forming Frenkel pairs. A typical low energy heat spike and resulting damage for FeCr with He defects are shown in Fig. 3.

The number of Frenkel pairs formed, and where they are formed in relation to each others, are important factors for determining the radiation resistance of a material. The damage caused by a displacement cascade will continue to evolve due to long time scale processes such as diffusion, but the damage formed during the first tens of picoseconds, the primary damage, will govern this evolution.

Another indicator of radiation resistance is the threshold displacement energy of a material. This is the amount of recoil energy needed to displace an atom from its lattice position. The threshold energy affects the size of the heat spike in a collision cascade, as well as determines Frenkel pair production due to recoil energies too low to cause a cascade.

4 METHODS

In this thesis, computational methods are used to study the basic properties, and irradiation, of materials. Computing power intensive *ab initio* calculations are used to improve the atomic interactions in molecular dynamics, which is used to study larger systems over a longer time scale. Performing calculations with different methods allows study on a larger scale, and the ability to compare results where the methods overlap.

4.1 Molecular dynamics

In molecular dynamics (MD) simulations, the equations of motion of all the atoms in the system are solved numerically. The forces between the atoms are calculated from a classical interatomic potential energy function, and the atoms are moved accordingly over a small time step. By repeating this, it is possible to simulate the time evolution of the system. Thermodynamic ensembles can be studied applying algorithms to control the temperature and pressure in the system. One of the great advantages of MD simulations is the atomic level detail available at all times.

With a short enough time step and accurate algorithms for solving the equations of motion, the calculational aspect of MD simulations is very precise. Whether the simulations describe reality depends on the potentials, the system size and time scale available within reasonable computation time, and how well the system can be described classically. While the properties of electronic, optical and magnetic phenomena can be mimicked with the interatomic potentials, they can not directly be simulated using classical MD. The reliability of MD simulations is discussed further in Sect. 4.1.1.

With present computing power it has become possible to perform MD simulations applying electronic structure calculations to obtain the motions of the atoms. It is, however, still limited to a small number of atoms and short time scales [50].

The MD simulations in this thesis were mostly carried out using the PARCAS code developed by Nordlund [51]. It applies the Berendsen temperature and pressure controls [52], a variable time-step, the GEAR5 predictor-corrector algorithm, as well as methods to remove heat at periodic boundaries and other features described in the thesis.

4.1.1 Modeling real materials

Perfectly describing phenomena in real materials is usually impossible in MD simulations, as well as other computational modeling. Length and time scale limits the system that can be studied. Today it is possible to simulate with millions of atoms and for nanoseconds, but the macroscopic systems of many experimental setups are still out of reach. The potentials themselves are often compromises, sacrificing accuracy in some properties in order to describe others well. When developing and using potentials, it is important to understand and critically assess which phenomena they are suitable for.

Another issue is that good potentials have not been developed for all interactions and desired properties. While acquiring the experimental and *ab initio* data needed to base the potentials on, and developing new potentials, is desirable, often it is not practically possible. If the existing potentials can describe the most important features, it can be possible to simulate the system leaving out non-essential elements. Thus for instance steel, which generally contains at least a dozen different elements, is presently impossible to model with all of them. Currently the approach is to focus on the main elements, for instance iron and chromium for ferritic steel. One must of course carefully consider any comparison between results for FeCr with results for real steels.

4.1.2 Interatomic potentials

For many of the materials studied in this thesis, several different potentials have been developed over the last decades. Discussing all possible options in detail would be excessive, as there are tens of different potentials for the studied elements and compounds. The choice of potentials has been based on careful consideration.

For the development of potentials for the W–C–H system, the existing potentials for the C–C, C–H and H–H interactions by Brenner were used. The potential formalism for these potentials is discussed in detail in Sect. 5.1.2. In MD, the only difference between isotopes of an element is the mass, as the chemical and physical binding to other atoms are mostly independent of the isotope, and the same potential can be used for the isotopes in MD simulations. Thus the same potential is used for hydrogen and deuterium in this thesis.

Most of the iron simulations in Sect. 7 use the Ackland–Mendelev (AMS) Fe–Fe potential [53]. It is generally considered to be good at describing defects and radiation damage. It is also the iron potential used in the FeCr potential by Olsson *et al.* [54], the so called two-band model (2BM). There are two versions of the 2BM, based on different sets of *ab initio* calculations. In this thesis the PAW version (based on plane augmented wave DFT) is used, but the two versions can be expected to

perform similarly at the studied concentration of 10% Cr. The Fe–He and Cr–He potentials developed in Sect. 5.2 are intended to work in conjunction with the 2BM. In addition a potential set for the Fe–Cr system by Chakarova *et al.* [55] is used for comparison in Sect. 7.1 and the Fe–Fe potentials by Dudarev *et al.* [56] and Finnis-Sinclair [57] in Sect. 5.2. For all He–He interactions, the pair potential by Beck [58] is used.

For the tungsten displacement cascade simulations in this thesis, three different W–W potentials were compared, the Ackland-Thetford (AT) potential [59], the Derlet *et al.* (D) potential [60], as well as the Juslin *et al.* (J) potential described in Sect. 5.1 and paper **I**. For the D potential, the repulsive part is by Björkas *et al.* [61]. For W–He, the potential by Henriksson *et al.* [62] was chosen over the old potential by Wilson [63]. This W–He potential was developed for describing He defect properties and migration in tungsten, but recent DFT results suggest that it overestimates the formation energies for the interstitial [16].

Most of the metal potentials used in this thesis are of the embedded-atom method (EAM) formalism [64, 65], or formalisms similar to it. The EAM formalism is generally considered good at describing metals, as it is a many-body potential that derives the potential energy of an atom “embedded” in an electron cloud, with the electron density at a certain point calculated based on the electron density of the atoms in the vicinity.

4.1.3 Simulation setup

For most of the simulations used for testing potentials, small simulation cells of a few thousand atoms were used, applying periodic boundary conditions. This is usually enough for describing mechanical properties and point defects, but tests were done for larger cells as well to ensure that the system sizes were large enough. The cohesive energies, bond lengths, defect formation energies and similar properties are given for cells equilibrated to zero temperature and pressure.

For all the FeCr simulations in this thesis, 10% Cr randomly distributed, designated as Fe–10Cr, was used. The simulation cells were created with the Fe and Cr atoms in body-centered cubic (BCC) lattice positions. While studying other compositions as well would be of interest, due to time constraints the focus is on the fusion reactor relevant conditions.

The simulations of small He and He–vacancy clusters in Sect. 6 were performed in $(10 \times a_0)^3$ cells, containing 2000 atoms before a cluster was inserted. Here a_0 is the lattice constant at the appropriate temperature. The simulations were run at 100–1800 K depending on which cluster was used, for

simulation times of up to 100 ns, until the statistics were sufficient. Both the PARCAS code and the DYMOKA [66] code were used.

In the cascade simulations in Sect. 7.2 and Sect. 7.3, a simulation cell was created with metal atoms in BCC positions and He either in interstitial or substitutional positions. The size of the cell was chosen to be large enough, so that the cascade would not overlap the periodic boundaries, which was ensured during the simulation by monitoring the kinetic energy of border atoms. The sizes used where $n \times n \times n \times a_0$ with n being 25, 31, 42 and 67 for 1 keV, 2 keV, 5 keV and 20 keV recoil simulations respectively. The number of atoms were $2n^3$ plus up to 1% interstitial He atoms, or more than 600 000 atoms for the largest simulations.

This initial configuration was equilibrated at 300 K and zero pressure. This temperature was chosen in order to compare with results for pure Fe[67, 68], FeCr [69–71] and W [61, 72]. As He is relatively mobile at these temperatures, the He atoms migrate around and form clusters. The microstructure will thus depend on the equilibration time. A simulation time of 25 ps was chosen, as the change in microstructure is fastest in the first 1–10 ps, and because an equilibration time of about 20–25 ps is needed after the recoil for the evolution of primary damage, thus allowing the He the same time to cluster before and after the introduction of the recoil.

After the initial equilibration, a recoil energy of 1 keV, 5 keV or 20 keV was given to a random metal atom in a random direction, however, chosen in such a way that the cascade would not get too close to the periodic boundaries. The heat spike was allowed to cool down and the primary damage to form for 25 ps. This was repeated for the same initial cell until sufficient statistics had been collected. The cascade simulations had constant volume, and temperature scaling at the borders to remove heat from the system, in order to simulate the features of a bulk material. For FeCrHe, where damage in the metal matrix is also formed due to the clustering of He, the simulations were repeated without introducing the recoil, in order to separate the clustering damage from that formed due to the cascade.

4.2 Density-functional theory

Density-functional theory (DFT), as discussed in more detail in Refs. [73, 74], consists of certain approximations in order to solve the Schrödinger equation for a system of atoms. The Born-Oppenheimer approximation, according to which the electrons will always find their ground state before the nuclei move, as they are much lighter and faster, is used to divide the Hamiltonian into fixed ions and moving electrons. DFT is based on the Hohenberg-Kohn theorems [75] stating that the electrons in the system can be described by an external potential from the ions, which only depends on the electron density and that the energy cannot be less than the energy of the ground state. The

other important basis for DFT is that we can use a Hamiltonian for non-interacting electrons with the interactions hidden in an effective potential, according to the Kohn-Sham ansatz [76].

In the end it is possible to solve the Schrödinger equation exactly, except for an exchange-correlation function $E_{xc}[\rho]$, which includes the approximations and depends on the electron density ρ. Several different forms of E_{xc} exist, one of the simplest being the local density approximation (LDA) [77], which assumes a locally homogenous electron density, and the generalized gradient approximation (GGA) [78–80], which uses gradients for the electron density.

One way to improve the accuracy and efficiency of the calculations is to describe the valence and core electrons with different functions. This is often used successfully in periodic systems. Using plane waves for the outer electrons works well, but the inner electrons are usually better described by spherical harmonic functions. The precision of the results depends on the number of plane waves used to describe the wave-functions of the valence electrons and the so called pseudo-potentials used for the core electrons.

5 POTENTIAL DEVELOPMENT

The development of a new potential is a demanding process of acquiring the data required to fit the potential to, choosing or developing the formalism best suited for the problem, finding the parameters for it, and testing the potential. A good understanding of the capabilities and limits of the potential formalism is needed, as well as a certain familiarity with the fitting techniques. Trying to fit all parameters to all the data at the same time rarely succeeds, and it is important to make good initial guesses for the parameters and fitting choices.

5.1 Tungsten-carbon-hydrogen

As described in Sect. 3.1.1, there is a lot of interest in studying deuterium properties in tungsten, carbon and tungsten carbide bulk and surfaces. Until this work, potentials existed only for some of the interactions needed to study the W–C–H system with MD simulations. As described in paper **I**, the development of potentials for this complex, ternary system required improved fitting methods, extensive testing and DFT calculations to extend the database of experimental and *ab initio* data from the literature.

Since their development, the potentials have been used in several studies in the W, WC and WCH systems [14, 18, 81–87]. In this thesis the W–W potential is used in the displacement cascade simula-

tions presented in section Sect. 7.3. Recently a W–W potential with improved point defect properties, but somewhat worse bulk properties, was developed with the same potential formalism [88]. It was, however, not fitted to work together with C–H and W–C. In addition, to include beryllium in the system, Be–Be, Be–C and Be–H potentials have recently been developed [89] and a Be–W potential is under development [90].

5.1.1 DFT calculations

In some cases the system of interest for the potential fitting has been studied, but with the focus on other properties than those needed for potential development. In particular, *ab initio* studies on molecules often include detailed geometrical and vibrational data, but not the cohesive energy, which is of utmost importance for potential development. For the tungsten hydride molecules WH_n, with 1,2,3,4 and 6 hydrogen atoms, the calculations by Wang and Andrews [91] were repeated, in order to obtain the energies. The GAUSSIAN 98 code [92] was used, with the BPW91 method [93, 94] and the 6-311++G(d,p) basis set for the hydrogen atoms and the SDD basis set for the tungsten atoms.

For W and WC, the known experimental structures and several hypothetical phases were studied. For tungsten, the phases were the dimer, diamond, simple cubic (SC), body-centered cubic (BCC) and face-centered cubic (FCC), and for tungsten carbide, they were the dimer, sodium chloride (NaCl), cesium chloride (CsCl), zincblende (ZnS), hexagonal WC, wurtzite and hexagonal WC_2. A spin-polarized GGA method, GGS-PW91 [78, 93] with a norm-conserving pseudopotential was used with the CASTEP code [95, 96]. To find the method and pseudopotential which describes the ground state best, extensive testing of the available options was performed.

At short interatomic distances, the fitted properties do not give an indication of how the potential should behave, as the atoms are too far from each other. The repulsive potential was modified with a smooth fit to a pair potential calculated for the dimers with DFT using the DMOL97 program package [97, 98]. Using hydrogenic orbitals [99], energy vs. distance in the repulsive region has been shown to be accurate [100, 101]. Instead of DFT data it would also be possible to use the theoretical model of the Ziegler-Biersack-Littmark (ZBL) universal potential [102]. The short range repulsive potential is important for simulations with higher energies, such as displacement cascades.

5.1.2 Potential formalism

The potentials for deuterium bombardment of W–C surfaces must be able to describe bulk, surfaces and molecules for all the elements, and both metallic and covalent bonding. They also need to be

reactive, *i.e.* able to break bonds. While many potential formalisms are excellent for a certain application, few are well suited for everything needed for the W–C–H system. There were a number of W–W [57, 59, 64, 103–105] and hydrocarbon potentials [106–110] available in the literature. Developing W–C and W–H potentials able to join the different formalisms of the metal and hydrocarbon potentials is not trivial.

The bond order potential (BOP) used by Brenner for hydrocarbons [106, 107] has, however, also been successfully applied to a metal carbide, PtC [111], as well as many other elements and compounds. Thus, while other options exist, it is reasonable to use a formalism with well known properties and fitting schemes, and for which much tested C–C, C–H and H–H potentials already exist, and develop new potentials for the W–W, W–C and W–H interactions.

Based on the original bond order concept by Pauling [112], and Abell's early work on the relation between bond length and bond energy [113], Tersoff developed the BOP formalism [114, 115] used here. Originally intended for covalent materials, it has since been successfully applied to molecules, metals and carbides, much due to a potent angle-dependent three-body term. The formalism has subsequently been updated and written in a slightly different notation, by Brenner for the hydrocarbon potentials used here, and more recently by Albe [111, 116, 117]. In the notation by Albe, the total energy is given by:

$$E = \sum_{i>j} f_{ij} \left[V_R^{ij}(r_{ij}) - \overline{b}_{ij} V_A^{ij}(r_{ij}) \right], \tag{1}$$

where f is a cutoff function that limits the potential to a computationally feasible interaction range.

$$f(r) = \begin{cases} 1, & r \leq R - D, \\ \frac{1}{2}\left(1 - \sin\frac{\pi(r-R)}{2D}\right), & |R - r| \leq D, \\ 0, & r \geq R + D \end{cases} \tag{2}$$

The bond-order term b is the defining feature of the formalism, as it includes both the angular and the coordination number dependence, as a sum over all neighboring atoms to a pair of atoms.

$$\overline{b}_{ij} = \frac{b_{ij} + b_{ji}}{2}, \tag{3}$$

$$b_{ij} = \left(1 + \sum_{k(\neq i,j)} f_{ik}(r_{ik}) g_{ik}(\theta_{ijk}) e^{2\mu_{ik}(r_{ij}-r_{ik})}\right)^{-1/2}, \tag{4}$$

where the angular dependent factor g is given by

$$g(\theta) = \gamma\left(1 + \frac{c^2}{d^2} - \frac{c^2}{d^2 + (h + cos\theta)^2}\right). \tag{5}$$

The repulsive and attractive potentials are of Morse type, with an additional S parameter:

$$V_R(r) = \frac{D_0}{S-1} e^{-\sqrt{2S}\beta(r-r_0)}, \tag{6}$$

$$V_A(r) = \frac{D_0 S}{S-1} e^{-\sqrt{\frac{2}{S}}\beta(r-r_0)}. \tag{7}$$

Three of the parameters of the formalism are directly associated to the dimer properties: the diatomic dissociation energy D_0, the diatomic equilibrium distance r_0, and β, which is related to the ground-state vibrational frequency. For this potential, the logarithm of the binding energy E_b vs. the bond length r_0 is linearly dependent, with the S parameter setting the slope. The γ parameter scales the bond-order term, 2μ sets the effect of different distances between neighboring atoms, while the c, d and h parameters set the type and strength of the angular dependence. The cutoff parameters R, which sets the cutoff range, and D, which affects the steepness of the cutoff, are usually best determined based on which neighbor atoms are to be included in the different structures.

5.1.3 Fitting methodology

As the purpose is to develop a potential that can be applied to study new and complicated phenomena, such as deuterium bombardment of WC surfaces, it must be as transferable and sturdy as possible. A method which has proven successful is fitting the potential to several real and hypothetical structures. A phase that is not stable enough to be observable experimentally, can still be studied with DFT. While the actual phase often is not of interest for further studies, it leads to a potential capable of realistically describing local configurations with similar coordination number, bond lengths and bond angles.

The potential is numerically fitted to a database of experimental and DFT values, such as bonding energes, bond lengths and elastic constants. As numerically fitting many parameters at once can be tricky, it is beneficial to make educated initial guesses for the parameters, and keeping some of them fixed. Thus the fitting will be an iterative process of fitting with different parameters, initial guesses and weights for the fitted properties.

This methodology has been successfully applied for several potentials [111, 117, 118]. Generally the fitting routine has included first neighbors only, but for W and WC it was extended to include different bond lengths in a structure, as the first and second neighbors in the BCC structure are close, and the cutoff would have to be steep in order not to include second nearest neighbors, and also because the W–W and W–C bonds in hexagonal WC are different.

For the WH molecules, a different approach had to be taken, as tungsten hydride does not form a bulk structure. The numerical fitting was modified to focus on the energetics and structures of the molecules. The properties of the H interstitial in W were further fitted by manually tweaking the parameters.

5.1.4 Potential testing

The fitted properties of both the W–W and W–C potentials are reproduced well, especially for the ground state phases. A binding energy vs. bond length comparison between the W–W BOP and DFT and experimental data, as well as some other W–W potentials is given in Fig. 4. For the other data, see paper **I**. As the focus was on describing WC well, some compromises had to be made for the W–W potential. The melting temperature is almost 1000 K lower than in experiments, and the vacancy formation energy is only half the experimental value. This deficiency is unfortunate, but not easily corrected without sacrificing other properties of the W–W potential and the WC system. The melting temperature of WC is excellently reproduced, and while the point defect properties are not experimentally well known, the BOP agrees with experiments in that C vacancies are energetically more favorable than W vacancies.

As the potentials are intended for bombardment of surfaces, the surface properties are obviously important. For tungsten, surface energies and structural parameters have been studied experimentally and theoretically. The BOP reproduces the surface structures well, though the surface energy is only half of that found in DFT. For WC, the comparison with DFT results is overall quite good, though the BOP underestimates the surface energies for most surfaces. DFT calculations of surface properties are, however, quite sensitive to system size and which methods are used. A more recent DFT study

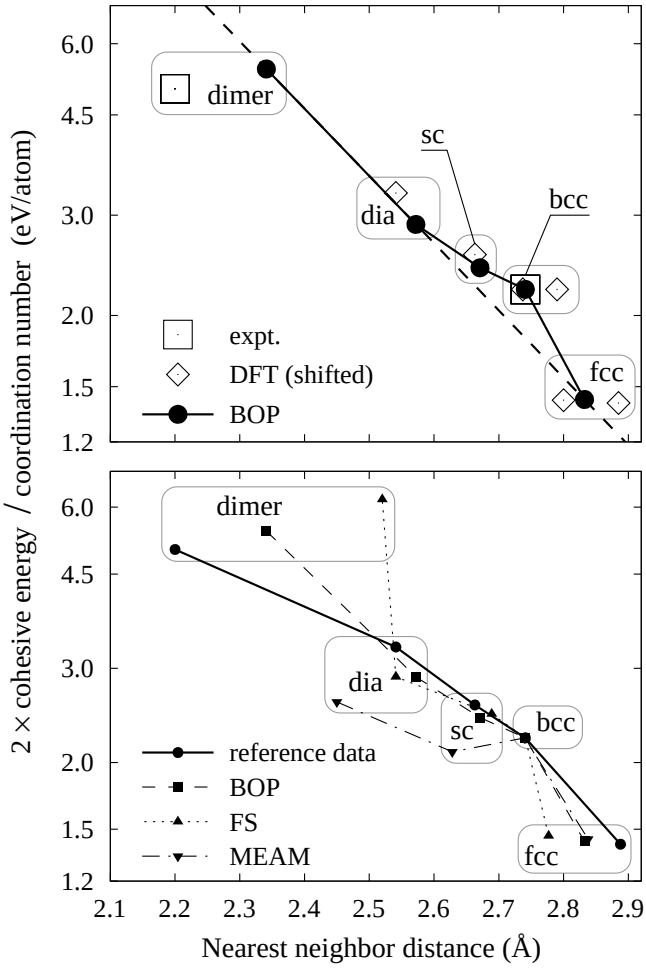

Figure 4: Bond energy vs. nearest neighbor distance for the W potential, compared with reference data and previous potentials. In contrast to a BOP with only first nearest neighbors, which would have a logarithmic dependence, the inclusion of second nearest neighbors allows the bump at the BCC structure and therefore a better description of all the phases.

[15] reports mostly similar results as the DFT results compared with in paper **I**, though there are also inconsistencies.

For tungsten hydride, the potential reproduces the smaller molecules, WH to WH_4, used for the fitting very well. WH_6, which was not used in the fitting, has several structures that are close in energy. The BOP ground state geometry and energy is a bit off from that in DFT, yet still reasonable. While it was possible to achieve a fit to the correct ground state, which has two different H–W–H angles for two triplets of W–H bonds, it deteriorated the other properties. Reconstruction of a hydrogenated surface is described well compared to experimental and DFT data. The potential describes the formation energy and position, as well as migration activation energy, of a hydrogen interstitial in tungsten very well, while the diffusion constant is wrong by about an order of magnitude. Overall, the potential works well for hydrogen both in bulk, on surfaces and for W–H molecules.

5.2 Iron-helium and chromium-helium

As helium is a noble gas, its properties in a metal can be described by a much simpler formalism than the formalism described in Sect. 5.1.2. In many metals, pair potentials have been used for the metal–He. Potentials for Fe–He [119] and W–He [63], which are relevant for this thesis, were created by Wilson in the 1970s. DFT calculations have, however, shown that these potentials do not describe the interstitial properties correctly [16, 37].

It has been suggested that the correct ground state for the He interstitial in Fe cannot be reproduced by a pair potential due to magnetic effects not included in conventional MD [120, 121]. Recently a many-body potential was developed for Fe–He by Seletskaia *et al.* [121, 122], with improved description of several properties. In paper **II**, we present a pair potential, which describes basic defect properties in accordance with DFT results, showing that a pair potential is capable of reproducing the correct ground state. In paper **III** a Cr–He potential is developed using the same potential formalism and methodology.

Both the Fe–He potential by Seletskaia *et al.* and the one presented here perform well, somewhat differing depending on the Fe–Fe potential and the properties studied. For further improvement, a many-body term might offer more options to tweak the potential to specific structures, while a pair potential allows easier implementation with Fe–Fe potentials using different formalisms. A pair potential is also computationally more efficient.

5.2.1 Data on He in Fe and Cr

For He in Fe, there is a generous amount of DFT data available in the literature. The basic defect structural and migrational properties have been studied by Fu and Willaime [37] and Seletskaia *et al.* [120–122]. As the Cr–He potential was developed, very little data on He in Cr existed in the literature, and thus DFT calculations for the basic properties were performed using the VASP code [123]. Qualitatively He behaves very similarly in Fe and in Cr, though the ground state of the He–V_2, a helium atom and two vacancy complex, is different. There are known issues with calculating the ground state of pure Cr with DFT [124, 125], and while calculations on the difference between states should be reliable, this constitutes an additional uncertainty in the results. In addition, the short range energies were acquired with *ab initio* dimer calculations, as described in Sect. 5.1.1.

5.2.2 Potential formalism and fitting

Due to the repulsive nature of the interactions of He in a metal, a natural form for a potential describing it is a screened Coulomb potential. For both the Fe–He and Cr–He potentials, the same function was used to describe the interaction, with the potential given by:

$$f(r) = (a + \frac{b}{r})e^{-cr} \tag{8}$$

Even with only one term, $f(r) = a\exp(-cr)$, it was possible to obtain a potential with adequate defect properties, but adding a b/r term allowed further fitting options and the possibility to affect different ranges of the potential. As for the W–C–H potentials in Sect. 5.1, a DFT dimer potential was used for the short range interactions. This was joined to the screened Coulomb functional form with a polynomial function. The same type of cutoff function as for the BOP in Sect. 5.1.2 was also used here. Including these, the full form of the potential was

$$f(r_{ij}) = \begin{cases} \text{DMol-potential}, & r_{ij} \leq r_1 \\ p_3 r_{ij}^3 + p_2 r_{ij}^2 + p_1 r_{ij} + p_0, & r_1 \leq r_{ij} \leq r_2, \\ \left(a + \frac{b}{r_{ij}}\right) e^{-cr_{ij}} f_c(r_{ij}), & r_{ij} \geq r_2, \end{cases} \tag{9}$$

with f_c given by Eq. 2.

A fitting routine was then constructed that could fit any function to any defect structure and energy. After numerically fitting to the defect properties, the parameters were tweaked manually to focus on the desired properties. In particular the cutoff length was derived by carefully considering which atoms were included in the interaction for certain He positions.

5.2.3 Potential testing

Both the Fe–He and Cr–He reproduce the fitted properties of the tetrahedral and octahedral interstitial and substitutional He. The migration energy barrier from a tetrahedral to tetrahedral position is excellently reproduced for Fe–He, while it is a bit high for Cr–He (see Fig. 5(a)). In addition to the Fe–Fe potential by Ackland-Mendelev, which the Fe–He potential was developed to be used with, two other Fe–Fe potentials were tested. The Dudarev-Derlet potential works well, though with slightly worse formation energies for the interstitial. With the Finnis-Sinclair potential, the migration barrier shows that the midpoint between the tetrahedral positions is actually more stable than the tetrahedral. Various properties with more than one He are discussed in Sect. 6, and have also been studied by others [49].

The migration of a substitutional He can be considered through the He–V_2 complex, with a He moving between two vacancies in nearest to third nearest neighbor positions. The energy landscape in Fig. 5(b) for Fe–He is DFT data from the literature [37], and for Cr–He three of the points were calculated with DFT. For Fe–He the overall agreement is quite good, though the barrier between nearest neighbors (positions e and f in Fig. 5(b)) is quite high, compared to DFT. For Fe–He the potential has a meta-stable state between the first nearest and second nearest positions, which is seen as a double peak. The literature DFT data, on the other hand, does not have enough points in that region to compare with. The stability of this state is, however, quite low compared with the height of the whole barrier. For Cr–He, the second nearest neighbor position is actually more stable than the first neighbor position according to DFT, while the potential gives a similar behavior to that for Fe–He. An effort to reproduce the DFT ground state was not made, as the accuracy of DFT calculations in Cr has been questioned, as discussed in Sect. 5.2.1.

6 HE AND HE–VACANCY CLUSTERS IN FE AND FECR

The formation, mobility and lifetimes of the He–vacancy clusters, studied in publication **III**, are very important for long time scale Monte Carlo (MC) studies of bubble formation and damage evolution of the primary damage formed in displacement cascades. Many of the parameters used for these

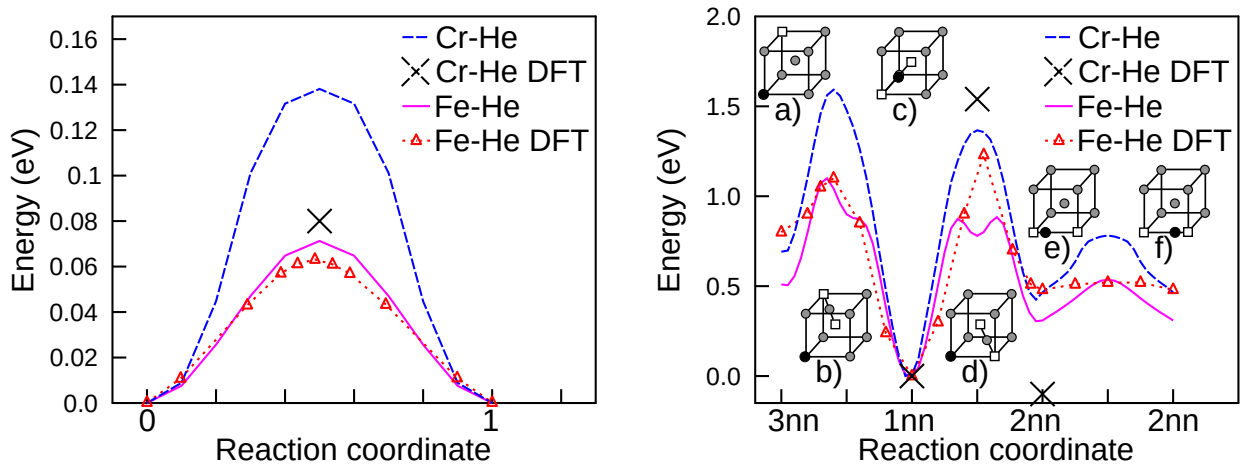

(a) (b)

Figure 5: Migration barriers for a He in Fe and a He in Cr, (a) the tetrahedral to tetrahedral position, and (b) a HeV_2 complex. For Cr only a few points were calculated with DFT. The DFT results for FeHe are from Ref. [37].

properties are, however, based on data with the old Fe–He potential, or on assumptions. Most models treat the clusters as immobile, without proper justification. Small, helium rich clusters, which could be mobile on a time scale available in MD, are studied with the recent potentials.

6.0.4 Cluster formation

The formation energies of point defects and small He–vacancy defects for Fe and Fe–10Cr are given in Fig. 6. Overall the formation energies are very similar for Fe and Fe–10Cr, but there are neighborhoods in the FeCr composition for which the formation energy can differ by up to 1 eV.

The binding and dissociation energy of a He or vacancy to a cluster was shown to depend strongly on the He/V ratio, and only weakly on the cluster size. As the ratio goes up, the binding and dissociation energies decrease for He and increase for the vacancy. The crossover where the He dissociation energy becomes less than for the vacancy is a He/V ratio of $\sim$1.1 and energy of $\sim$2.4 eV, which corresponds well with a ratio of $\sim$1.3 and energy of $\sim$2.6 eV with DFT [37, 40]. The Wilson Fe–He potential has a significantly higher crossover ratio and energy [37]. While there are small differences for some clusters, overall the presence of 10% Cr does not significantly affect the binding and dissociation of He and vacancies to small clusters.

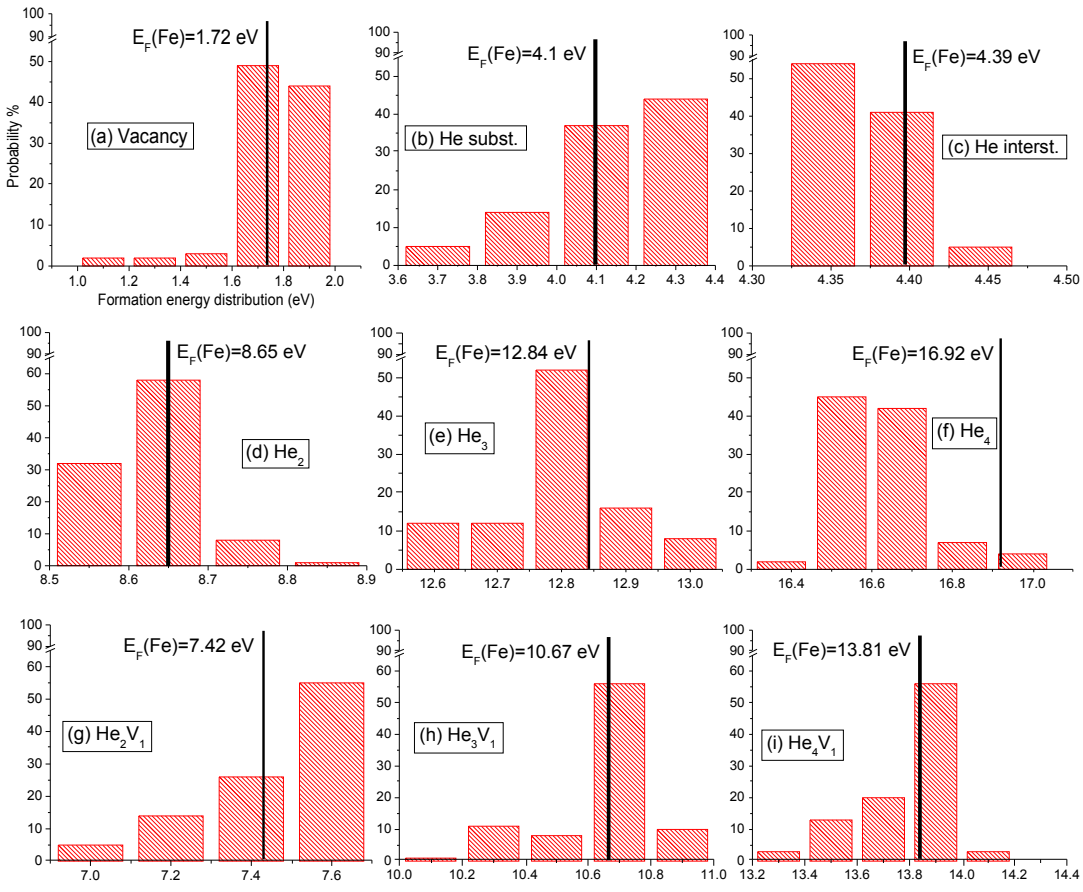

Figure 6: The probability distributions for the formation energy of He defects in Fe (black bar) and Fe–10Cr (shaded box). Overall the most probable energy for FeCr is close to the result for pure Fe, but in some cases there are significant differences, in particular for He_4 (f) and He_2V_1 (g).

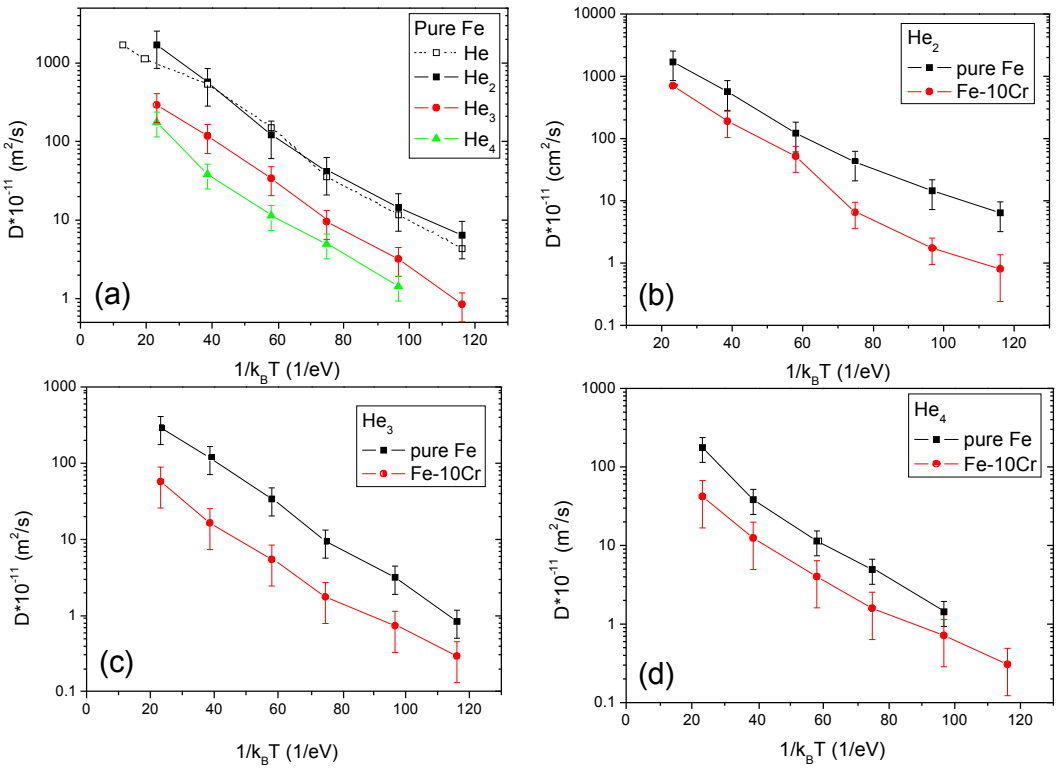

Figure 7: The diffusion coefficients for He_{1-4} clusters in pure Fe and FeCr with 10% Cr. In (a) the diffusion is compared between clusters of different sizes, while in (b)-(d) it is compared between pure Fe and FeCr.

6.0.5 The mobility and lifetime of clusters

In particular the pure He clusters were found to be very mobile. The migration energies of the clusters are similar to that of a single He interstitial, and the migration mechanism is the same, with individual He atoms jumping from one interstitial position to another in three dimensions. The diffusion constants vs. temperatures for the different clusters are shown in Fig. 7. The presence of 10% Cr slightly reduces the mobility of the clusters.

The He–vacancy clusters are less mobile than the pure He clusters, however, still more mobile than a single vacancy. The effect of Cr is statistically insignificant in this case. The He_n–V_1 clusters migrate by temporarily pushing away a metal atom, creating a He_n–V_2 cluster, after which the metal atom recombines with one of the vacancies, thus allowing 3D motion of the cluster. As the migration energies of the clusters, about 0.3 eV, are close to the migration energy for the Fe self-interstitial atom (SIA), it can be assumed that the mechanism is governed by the SIA migration. The He_2–V_3 cluster was found to perform a ring like diffusion with the mechanism controlled by single vacancy diffusion. The diffusion of several different defect types in Fe are compared in Fig. 8.

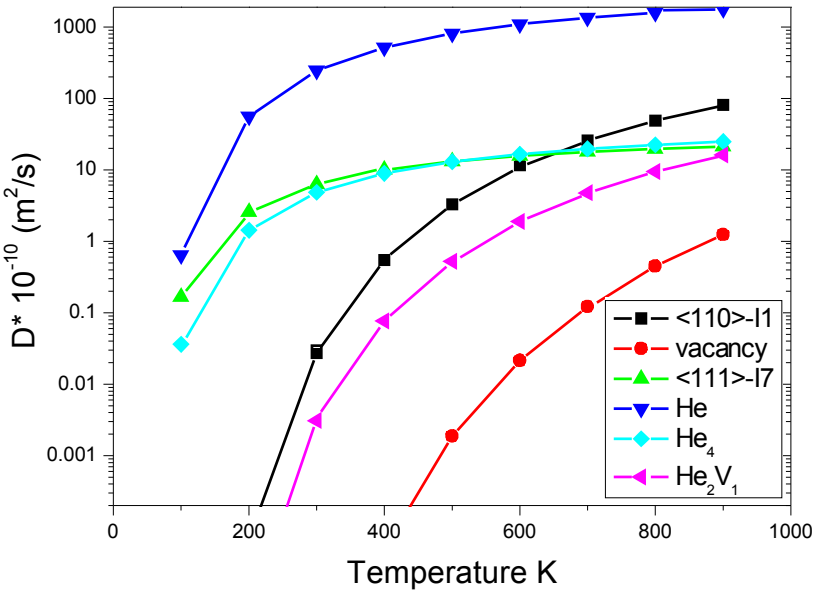

Figure 8: A comparison of diffusion for different defects and defect clusters in pure iron. <110>-I1 is the self-interstitial in the <110> dumbbell configuration, and <111>-I7 a cluster with 7 SIAs from Ref. [126].

The clusters can dissociate by emitting helium atoms. Usually, the Debye frequency of Fe is used for the dissociation attempt frequency of the clusters in MC studies. This study, however, shows that the attempt frequency can be up to two orders of magnitude higher for some of the clusters; for the He_3–V cluster it is even three orders of magnitude higher. Thus the previously often assumed properties for both the mobility and dissociation of small He and He–vacancy clusters are shown to be unjustified, and long–time scale damage evolution models will have to be justified accordingly.

7 IRRADIATION SIMULATIONS

7.1 Threshold displacement energies in FeCr

The threshold displacement energy, which is the minimum recoil energy needed to displace an atom from its lattice position to produce a Frenkel pair, is one of the basic properties of radiation resistance. It depends on the lattice direction and usually there is a minimum in one direction, which is clearly lower than the average threshold energy. A comparison of 11 iron potentials was made by Nordlund *et al.* [127], where they in detail discussed different definitions of threshold energy and the comparison of simulations and experiments.

Table 1: Threshold displacement energies for Fe, Cr and FeCr. The element in parenthesis is the element which got the recoil energy. All energies are given in eV. The accuracy is $\pm$ 1 eV for the values for the threshold energies in the 100, 110 and 111 crystal directions.

	Potential	$N_{directions}$	$E_d(\theta,\phi)$				$E^{av}_{d,ave}$	$E^{av}_{d,med}$
			all	100	110	111		
Fe	Chakarova	2386	19	19	47	29	53.5 $\pm$ 0.5	53
	Olsson[a]	3655	15	15	33	35	39.3$\pm$ 0.3	35
	Experiments[b]		16-18	17	>30	20		
Cr	Chakarova	3250	15	15	33	27	43.2$\pm$0.4	43
	Olsson	2420	21	21	55	31	56.2$\pm$0.5	53
FeCr	Chakarova(Fe)	2657	21	21	53	29	52.4$\pm$0.5	51
	Chakarova(Cr)	2077	17	17	39	29	53.4$\pm$0.6	53
	Olsson(Fe)	1491	15	15	33	39	39.1$\pm$0.5	35
	Olsson(Cr)	4309	17	17	37	33	40.7$\pm$ 0.3	37

[a] The Fe-Fe interaction is the Ackland-Mendelev potential [53]
[b] References [128–130].

In paper **IV**, the threshold energies for FeCr with 10% Cr and pure Cr were compared with results for pure Fe for two different Fe–Cr potential sets, the 2BM and the potentials by Chakarova *et al.* (Table 1). The differences in threshold energies between the potentials are rather large for all the studied compositions. The average and median threshold energies differ in the range 35–55 eV. The potentials do agree that the 1 0 0 lattice direction has the lowest threshold energy in all cases, with an energy of 15-21 eV, which is also seen experimentally for pure iron [128–130].

There is a significant disparity in the results for pure Fe and pure Cr, and it is interesting to note that the 2BM Fe threshold energies are closer to those for Chakarova Cr than for Fe. The results for FeCr with 10% Cr are, however, very close to those in pure Fe, both with Fe and Cr recoil atoms, though the thresholds for a Cr recoil tend a bit towards those in pure Cr.

Just as for displacement cascades, as discussed in the following section, the effect of 10% Cr on threshold energies does not explain the observed dependence on Cr seen on mechanical properties in irradiated FeCr discussed in Sect. 3.1.2. It can be concluded that the primary damage is unaffected by the Cr, and that the effect must be due to long time scale evolution of the damage.

7.2 The effect of He on cascades in FeCr

Simulations of displacement cascades in pure iron and FeCr with 5–15% Cr have been studied extensively in the literature [67–71, 131]. There are a few studies [35, 132–134] of cascades in Fe with 0.1-1% He using the old Fe–He potential by Wilson, as well as one recent study [135] using

the Fe–He potential developed in Sect. 5.2. In short, about 10% Cr does not affect the total amount of cascade damage in FeCr, and He, especially at a concentration of 1%, can significantly affect the damage production. Whether the presence of both Cr and He has an effect on cascades was studied in paper **V** and is discussed below.

Depending on the He concentration, a certain amount of He clustering will take place during the equilibration both before and after the cascade. A 25 ps equilibration at 300 K and zero pressure will not lead to any large clusters for 0.1% interstitial He, and most He atoms will remain as single interstitials. For the higher concentrations, small He bubbles form, containing up to tens of He atoms. As more than 3-4 He cluster together, they can force a metal atom to leave its lattice point, forming a Frenkel pair.

While 10% Cr does not on average affect the formation of small clusters, as shown in Sect. 6, Cr plays a role in micro-structure evolution, as the He atoms tend to migrate away from Cr atoms. Thus the He clusters mainly form in iron rich regions. The amount of Cr within the first 0.5–1.5 a_0 of a He atom is much lower than the 10% of metal atoms in a random solution, as shown in Fig. 9(a). The He clusters lead to high local concentrations of He within the nearest 2 a_0 of a He atom, but within distances longer than 3 a_0, the concentrations are the same as the He concentration of the whole system (Fig. 9(b)).

7.2.1 Damage production

By examining the occupancy of the Wigner-Seitz cells, vacancies, interstitials and substitutional He were located. As shown in Fig. 10(a), He can affect the Frenkel pair production. With 0.1% interstitial He, no effect on total damage is seen, but at higher He concentrations the damage is increased quite significantly, especially for the 5 keV cascades, where the number of Frenkel pairs for the 1.0% He case is almost quadruple that in pure FeCr. As vacancies are formed during the cascade, some combine with He to form substitutional He or He–vacancy clusters, thus reducing the vacancies available for recombination with metal atoms. All but a few of the vacancies produced in the cascade will be filled with one or more He atoms, as shown in Fig. 10(b).

The amount of Frenkel pairs is also higher in FeCrHe than in FeHe [135]. The methods used for FeHe were, however, not identical to those for FeCrHe. In particular, the equilibration time before the cascade was much shorter, 1-2 ps, and thus the micro-structure of He in the metal matrix was different. Recent unpublished results indicate that the micro-structure affects the damage production more than the presence of 10% Cr.

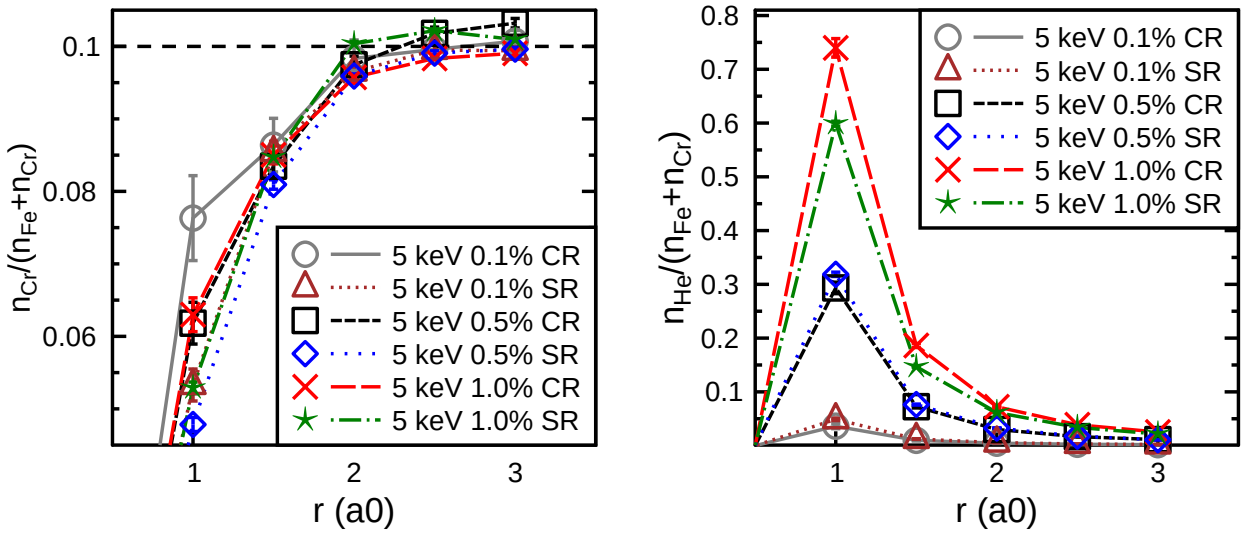

(a) (b)

Figure 9: (a) The concentration of Cr among metal atoms in the vicinity of a He atoms, averaged over all He atoms in the system. The concentration is a bit higher inside the cascade region. (b) The concentration of He among metal atoms in the vicinity of a He atoms, averaged over all He atoms in the system. The concentration is a bit higher inside the cascade region.

In order to further analyze the cascade, the simulation cell is divided into a cascade region (CR), and the surrounding region (SR), with the CR consisting of the part of the cell that was molten during the peak of the heat spike and the atoms adjacent to this part, with a simple kinetic energy criteria for an atom being part of the molten region. An interesting result is that the amount of He in the cascade region is increased due to the cascade. The increase is about 30%, though the variation from case to case can be quite high, in particular for low energies and He concentrations, as there are just a few He atoms in the cascade region. A likely cause for this is that the vacancies produced in the cascade trap He atoms, which cause more He to migrate into the cascade region than out of it.

With the He in substitutional positions initially, the number of Frenkel pairs produced is reduced. In a 5keV cascade with 1% substitutional He only a few Frenkel pairs are produced, compared with $\sim$15 for pure FeCr. This is explained by the fact that during the cascade, some He atoms end up as interstitial He and in larger He–vacancy clusters, and the metal interstitials have a higher concentration of vacancies to recombine with.

Based on these results, the following conclusions can be made. Several factors will govern the resulting primary damage in a real, prolonged irradiation of FeCr with He defects. As the He concentration in the cascade region increases, the micro-structure formation is enhanced. The micro-structure is

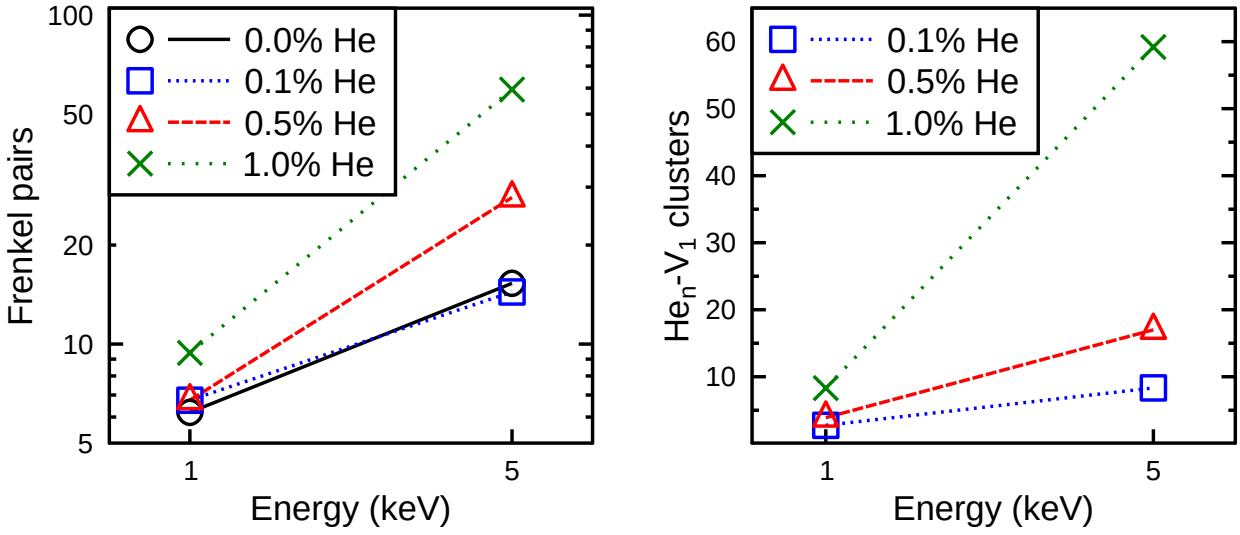

(a) (b)

Figure 10: The damage produced by cascades in FeCr with different He concentrations and recoil energies. In (a) the number of Frenkel pairs, and in (b) the number of He–vacancy clusters are shown.

likely to affect the amount of damage, possibly to a large extent. He in interstitial positions or small clusters increase the damage production, while He in substitutional positions decrease it and cumulative cascades can be expected to reach an equilibrium. Finally, further studies of how the He, and FeCr, micro-structure affects cascade damage promise to be very interesting.

7.3 The effect of He on cascades in W

The W divertor will contain He, both due to He bombardment from the plasma, and transmutation reactions. Most of the ions from the plasma have very low energy, but the divertor will be subject to some ions energetic enough to cause cascade damage, as well as the high energy neutron irradiation all reactor materials suffer from. Thus it is of interest to study how He affects displacement cascades in W. As W, Fe and FeCr are BCC metals, the effect can be expected to be similar to that in Fe and FeCr. There are, however, large differences in material properties, and in the pure materials, the amount of damage is much smaller in W. A comparison of different W–W potentials, the Ackland-Thetford (AT), Derlet *et al.* (D) and Juslin (J) potentials described in Sect. 4.1.2 and the effect of He on cascades was performed in paper **VI**.

First the basic interstitial and substitutional He formation energies were compared between the poten-

Table 2: The fraction of vacancies (V) and self-interstitials (SI) that are in clusters, as described in the text, for 2 keV cascades. The He atoms were initially in interstitial positions. The results for pure W are, for the Derlet *et al.* (D) potential from Ref. [61] and for the Ackland-Thetford (AT) and Juslin (J) potentials from Ref. [72].

	AT		D		J	
	Pure	1.0% He	Pure	1.0% He	Pure	1.0% He
V	0.28±0.04	0.04±0.01	0.24±0.08	0.23±0.02	0.22±0.04	0.07±0.01
SI	0.24±0.04	0.20±0.03	0.31±0.07	0.29±0.02	0.24±0.04	0.20±0.01

tials, and the most recent DFT results. The formation energy is overestimated in all cases compared to DFT [16], except for the substitutional He for the J potential, due to the low vacancy formation energy with this potential. The formation energy of the interstitital is relatively high both in the MD simulations and in DFT, 7.8–9 eV and 6.2–6.5 eV respectively. This discrepancy can affect the cascade damage, and development of a new W–He potential should be considered for future studies.

7.3.1 Damage production

As can be expected, the same mechanics that govern the effects of interstitial and substitutional He described in Sect. 7.2.1 for FeCr, are found for tungsten. The total damage, and the increase in damage due to interstitial He, is less than in FeCr, though the smaller effect of He can partially be attributed to the difference in micro-structure. Studying the effect of the micro-structure is certainly of interest for future studies.

A recoil energy of 2 keV is the highest energy, for which pure W has been studied for all the potentials. As the effect of He can be expected to be more pronounced at higher energies, the potentials were compared for this recoil energy. Both the amount of damage and the clustering of vacancies and interstitials, are relatively similar, with the amount of Frenkel pairs and interstitial clustering slightly higher for the potential by Derlet *et al.* than for the others as can be seen in Fig. 11(a) and Table 2. For substitutional He, the amount of damage compared with pure W is reduced for 1% He, while it is unchanged for 0.1%, except for the W–W potential from Sect. 5.1, for which it is a bit higher. While there are apparent differences between the potentials, the qualitative features of the damage are the same.

For the D potential, higher energy recoils have been simulated. As can be seen in Fig. 11(b), the damage production increases exponentially with recoil energy, as it does for pure W. The slope of the fitted curve in a log-plot remains the same with 1% interstitial He as for pure W. The damage production with 5 keV recoil with 0.1% He is surprisingly very similar to that with 1% He. Even for

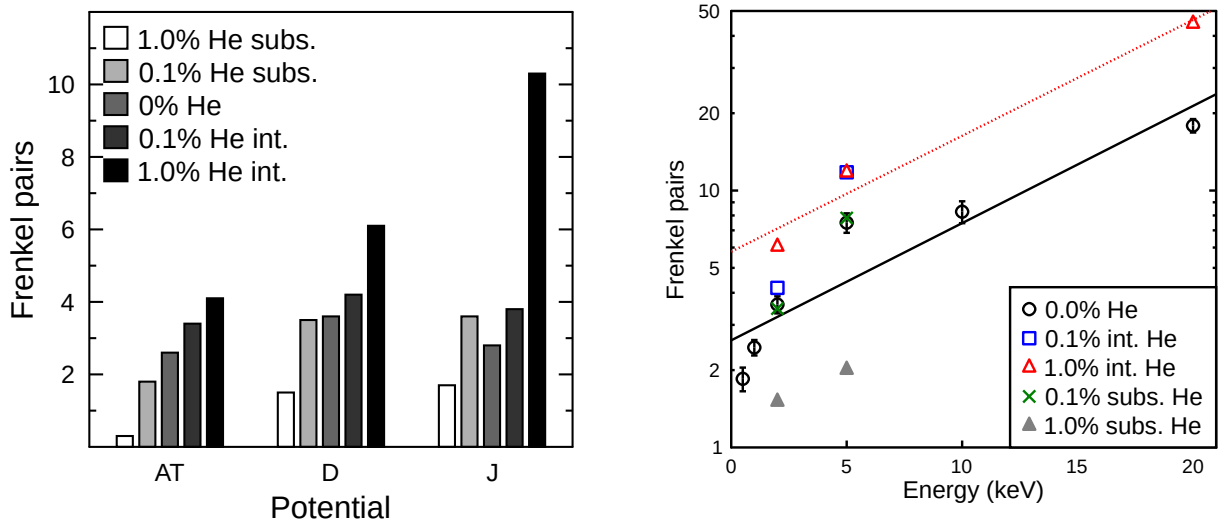

(a) (b)

Figure 11: The damage produced by cascades in W with different He concentrations and recoil energies for both interstitial (int.) and substitutional (subs.) He. In (a) the number of Frenkel pairs are compared for the Ackland-Thetford (AT), Derlet *et al.* (D) and Juslin (J) W–W potentials. In (b) the number of Frenkel pairs for 2, 5 and 20 keV recoils for the D potential. The results for 0% He are from Ref. [61] for the D potential and from Ref. [72] for the AT and J potentials.

pure tungsten, the 5 keV recoil produces a high amount of damage compared to other energies. With substitutional He, the amount of damage is reduced for 1% He, especially in the 5 keV case, where the number of Frenkel pairs is reduced to about a quarter of that in pure W. For 0.1% the damage is unchanged.

8 CONCLUSIONS

In this thesis, interatomic potentials needed for molecular dynamics simulations of irradiation of materials have been developed and applied. The focus is on the fusion reactor relevant materials tungsten and iron chromium, and the deuterium bombardment of tungsten and effects of helium in both tungsten and iron chromium. While the motivation for the work was to study materials for future fusion reactor applications, the research leans towards study of the basic science behind the phenomena, rather than an engineering approach.

New potentials have been developed for the W–W, W–C and W–H interactions, based on data from both literature and *ab initio* calculations in this thesis. While the potentials have certain known shortcomings, they perform well for their intended use and they are still the only potential set for simulating a WCH system. The W–C and W–H potentials are not used further in this thesis, but have been applied by several groups for a wide range of studies.

Pair potentials able to describe He defect properties in Fe and Cr were developed in order to study the effect of He on irradiation properties in Fe and FeCr, as model materials for fusion reactor steels. The potentials are able to describe the interstitial and substitutional energies very well, as well as migrational properties adequately. The Fe–He potential has also been widely used and tested by others. For the Cr–He potential, the lack of known experimental or *ab initio* data limits the testing possibility. There are, however, groups performing *ab initio* studies of He in Cr and FeCr and it remains to be seen how well the potential can reproduce those results.

The presence of 10% Cr does not greatly affect the formation, mobility and lifetime of He and He–vacancy clusters. The formation energy can be quite different depending on the local neighborhood, but on average cluster formation, as well as the binding to and dissociation from a cluster, of a He or vacancy, is not significantly affected by Cr. The mobility of pure He clusters is retarded by a small degree due to 10% Cr. The mobility and dissociation frequency of the clusters were shown to be higher than previously assumed, in some cases several orders of magnitude.

The effect of Cr on the displacement threshold energies in FeCr with 10% Cr was shown to be negligible. There is a small difference on whether the displaced atom is Cr or Fe, but even for the Cr atom, the results are close to those for a Fe atom in pure Fe. On the other hand, there are considerable differences between the results for FeCr and pure Cr. Together with the results that Cr hardly affects the total damage in displacement cascades in FeCr, this indicates that the experimentally observed effect that the dependence on Cr on the irradiation response of FeCr most likely comes from long time scale damage evolution and is not due to primary damage formation.

A concentration of 0.5-1% interstitial He significantly increases the displacement cascade damage production, while He in substitutional positions reduces it. This is seen both in FeCr and W. At lower concentrations the primary damage production is not notably different than for the pure materials. The increase due to interstitials is explained by He atoms combining with vacancies produced during the cascade, thus reducing the recombination of metal atoms and vacancies. The reduction due to substitutional He has the opposite mechanism, as some of the He become interstitial or clusters, leaving more vacancies for the metal interstitials to recombine with.

All of the studies performed on FeCr and FeCrHe in this thesis indicate that 10% randomly distributed Cr influences the primary damage production or He migration and clustering to an insignificant degree. Helium,on the other hand, can greatly increase the amount of primary damage, but only for concentrations that approach the limit of what is expected to be produced during the lifetime of a reactor. Also in tungsten a similar effect of He is seen. Local variations in concentration and microstructure of He could, however, play a significant role in a real material and are certainly of interest for further studies.

ACKNOWLEDGMENTS

I wish to thank the head of the Department of Physics at the University of Helsinki, Professor Juhani Keinonen, as well as the head of the Accelerator Laboratory, Professor Jyrki Räisänen, for providing me with an excellent and exciting place to study and conduct my research, all the way from my first stumbling steps as a physicist to a doctoral degree.

I especially wish to thank my supervisor Professor Kai Nordlund, without whom I would not be here today. You took me into the group with open arms and have provided me with an interesting and encouraging field of research. You have both guided me and allowed me to figure things out on my own, making a materials scientist out of me.

I am grateful to have so many great co-workers and friends at the Accelerator Laboratory. In particular, I wish to thank Toffe, Caro, Tommi, Jani and Eero for being amazing friends.

Several collaborators at other laboratories have made this research possible, as well as being excellent hosts while visiting them. I also wish to thank my co-workers and friends at Lawrence Livermore National Laboratory for giving me a wonderful summer institute filled with experiences.

Many thanks are due to my family and friends, who have always been there to support me. All the wonderful people in Spektrum have made it a second home for me all these years.

Marie, thank you for everything!

Helsinki, October 2, 2009
Niklas Juslin

References

1. ITER Physics Basis Editors, ITER Physics Expert Group Chairs and Co-Chairs and ITER Joint Central Team and Physics Integration Unit, *ITER Physics basis*, Nuclear Fusion **39**, 2137 (1999).

2. Progress in the ITER Physics Basis editors, *Progress in the ITER Physics Basis*, Nuclear Fusion **47**, 1 (2007).

3. The official ITER webpage: http://www.iter.org/.

4. H. Plank and W. Eckstein, *Preferential sputtering of carbides under deuterium irradiation - a comparison between experiment and computer simulation*, Nucl. Instr. Meth. Phys. Res. B **124**, 23 (1997).

5. E. Salonen, K. Nordlund, J. Keinonen, and C. H. Wu, *Carbon erosion mechanisms in tokamak divertor materials: insight from molecular dynamics simulations*, J. Nucl. Mater. **290-293**, 144 (2001).

6. E. Salonen, K. Nordlund, J. Keinonen, and C. H. Wu, *Swift chemical sputtering of amorphous hydrogenated carbon*, Phys. Rev. B **63**, 195415 (2001).

7. E. Salonen, K. Nordlund, J. Keinonen, and C. H. Wu, *Molecular dynamics studies of the sputtering of divertor materials*, J. Nucl. Mater. **313–316**, 404 (2003).

8. P. Träskelin, E. Salonen, K. Nordlund, J. Keinonen, and C. H. Wu, *Molecular dynamics simulations of CH_3 sticking on carbon surfaces, angular and energy dependence*, J. Nucl. Mater. **334**, 65 (2004).

9. K. Nordlund, E. Salonen, A. V. Krasheninnikov, and J. Keinonen, *Swift chemical sputtering of covalently bonded materials*, Pure and Applied Chemistry **78**, 1203 (2006).

10. J. Amano and D. N. Seidman, *Diffusivity of ^{3}He atoms in perfect tungsten crystals*, J. Appl. Phys. **56**, 983 (1984).

11. R. A. Causey, *Hydrogen isotope retention and recycling in fusion reactor plasma-facing components*, J. Nucl. Mater. **300**, 91 (2002).

12. K. O. E. Henriksson, K. Nordlund, and J. Keinonen, *Molecular dynamics simulations of helium cluster formation in tungsten*, Nucl. Instr. Meth. Phys. Res. B. **244**, 377 (2005).

13. K. O. E. Henriksson, K. Nordlund, A. Krasheninnikov, and J. Keinonen, *The depths of hydrogen and helium bubbles in tungsten - a comparison*, Fusion Science & Technology **50**, 43 (2006).

14. K. O. E. Henriksson, K. Vörtler, S. Dreißigacker, K. Nordlund, and J. Keinonen, *Sticking of atomic hydrogen on the tungsten (001) surface*, Surf. Sci. **600**, 3167 (2006).

15. F. Marinelli, A. Jelea, and A. Allouche, *Interactions of H with tungsten carbide surfaces: An ab initio study*, Surface Science **601**, 578 (2007).

16. C. S. Becquart and C. Domain, *Ab initio calculations about intrinsic point defects and He in W*, Nucl. Instr. Meth. Phys. Res. B **255**, 23 (2007).

17. C. S. Becquart and C. Domain, *A density functional theory assessment of the clustering behaviour of He and H in tungsten*, J. Nucl. Mater. **386-388**, 109 (2009).

18. Ohya, Y. K., Kikuhara, K. Inai, A. Kirschner, D. Borodin, A. Ito, H. Nakamura, and T. Tanabe, *Simulation of hydrocarbon reflection from carbon and tungsten surfaces and its impact on codeposition patterns on plasma facing components*, J. Nucl. Mater. **390-391**, 72 (2009).

19. S.-C. Lee, J.-H. Choi, and J. G. Lee, *Energetics of He and H atoms with vacancies in tungsten: First-principles approach*, J. Nucl. Mater. **383**, 244 (2009).

20. K. Ehrlich, E. E. Bloom, and T. Kondo, *International strategy for fusion materials development*, J. Nucl. Mater. **283-287**, 79 (2000).

21. L. Malerba, D. A. Terentyev, G. Bonny, A. V. Barashev, C. Björkas, N. Juslin, K. Nordlund, C. Domain, P. Olsson, N. Sandberg, and J. Wallenius, *Modelling of Radiation Damage in Fe-Cr Alloys*, J. ASTM Int. **4**, 100692 (2007).

22. S. Dudarev, J.-L. Boutard, R. Lässer, M. Caturla, P.M.Derlet, M. Fivel, C.-C. Fu, M. Lavrentiev, L. Malerba, M. Mrovec, D. Nguyen-Manh, K. Nordlund, M. Perlado, R. Schäublin, H. V. Swygenhoven, D. Terentyev, J. Wallenius, D. Weygand, and F. Willaime, *The EU programme for modelling radiation effects in fusion reactor materials: An overview of recent advances and future goals*, J. Nucl. Mater. **386-388**, 1 (2009).

23. P. Spätig, G. R. Odette, G. E. Lucas, and M. Victoria, *On the mechanical properties of the advanced martensitic steel EUROFER 97*, J. Nucl. Mater. **307-311**, 536 (2002).

24. J.-L. Boutard, M. J. Caturla, S. L. Dudarev and F. Willaime, *Strategic Objectives for Fusion Materials Modelling and Experimental Validation (2010-2015)*, EFDA Report (2009), official EFDA web-page: http://www.efda.org/.

25. R. A. Jameson, R. Ferdinand, H. Klein, J. Rathke, J. Sredniawski, and M. Sugimoto, *IFMIF accelerator facility*, J. Nucl. Mater. **329-333**, 193 (2004).

26. A. Kohyama, A. Hishinuma, D. S. Gelles, R. L. Klueh, and K. Ehrlich, *Low-activation ferritic and martensitic steels for fusion application*, J. Nucl. Mater. **233-237**, 138 (1996).

27. S. I. Porollo, A. M. Dvoriashin, A. N. Vorobyev, and Y. V. Konobeev, *The microstructure and tensile properties of Fe-Cr alloys after neutron irradiation at 400*deg*C to 5.5-7.1 dpa*, J. Nucl. Mater. **256**, 247 (1998).

28. B. H. Sencer and F. A. Garner, *Compositional and temperature dependence of void swelling in model Fe-Cr base alloys irradiated in the EBR-II fast reactor*, J. Nucl. Mater. **283-287**, 164 (2000).

29. R. Klueh, K. Ehrlich, and F. Abe, *Ferritic/martensitic steels: promises and problems*, J. Nucl. Mater. **191-194**, 116 (1992).

30. H. Ullmaier, in *Atomic defects in metals*, Vol. 25 of *Landolt-Börnstein, New Series III*, edited by H. Ullmaier (Springer, Berlin, 1991), Chap. 3.

31. J. Henry, M.-H. Mathon, and P. Jung, *Microstructural analysis of 9% Cr martensitic steels containing 0.5 at.% helium*, J. Nucl. Mater. **318**, 249 (2003).

32. P. Jung, J. Henry, J. Chen, and J.-C. Brachet, *Effect of implanted helium on tensile properties and hardness of 9% Cr martensitic stainless steel*, J. Nucl. Mater. **319**, 241 (2003).

33. R. Sugano, K. Morishita, A. Kimura, H. Iwakiri, and N. Yoshida, *Microstructural evolution in Fe and Fe-Cr model alloys after He^+ ion irradiation*, J. Nucl. Mater. **329-333**, 942 (2004).

34. K. Ono, K. Arakawa, H. Shibasaki, H. Kurata, I. Nakamichi, and N. Yoshida, *Release of helium from irradiation damage in Fe-9Cr ferritic alloy*, J. Nucl. Mater. **329-333**, 933 (2004).

35. R. Schäublin and Y. L. Chiu, *Effect of helium on irradiation-induced hardening of iron: A simulation point of view*, J. Nucl. Mater **362**, 152 (2007).

36. R. Schäublin, J. Henry, and Y. Dai, *Helium and point defect accumulation: (i) microstructure and mechanical behaviour*, C. R. Physique **9**, 389 (2008).

37. C. Fu and F. Willaime, *Ab initio study of helium in α-Fe : Dissolution, migration, and clustering with vacancies*, Phys. Rev. B **72**, 064117 (2005).

38. K. Morishita and R. Sugano, *Mechanism map for nucleation and growth of helium bubbles in metals*, J. Nucl. Mater. **353**, 52 (2006).

39. L. Ventelon, B. Wirth, and C. Domain, *Helium-self-interstitial atom interaction in α-iron*, J. Nucl. Mater. **351**, 119 (2006).

40. C. Fu and F. Willaime, *Interaction between helium and self-defects in α-iron from first principles*, J. Nucl. Mater. **367-370**, 244 (2007).

41. C. J. Ortiz, M. J. Caturla, C. C. Fu, and F. Willaime, *Impurity effects on He diffusion in α-Fe*, J. Nucl. Mater. **368-388**, 33 (2009).

42. J.-H. Shim, S. C. Kwon, W. W. Kim, and B. D. Wirth, *Atomistic modeling of the interaction between self-interstitial dislocation loops and He in bcc Fe*, J. Nucl. Mater. **367-370**, 292 (2007).

43. K. Morishita, R. Sugano, B. D. Wirth, and T. Diaz de la Rubia, *Thermal stability of helium-vacancy clusters in iron*, Nucl. Instr. Meth. Phys. Res. B **202**, 76 (2003).

44. K. Morishita, R. Sugano, and B. D. Wirth, *MD and KMC modeling of the growth and shrinkage mechanisms of helium-vacancy clusters in Fe*, J. Nucl. Mater. **323**, 243 (2003).

45. B. D. Wirth and E. M. Bringa, *A Kinetic Monte Carlo Model for Helium Diffusion and Clustering in Fusion Environments*, Physica Scripta **T108**, 80 (2004).

46. K. Morishita and R. Sugano, *Modeling of He-bubble migration in bcc Fe*, Nucl. Instr. Meth. Phys. Res. B **255**, 52 (2007).

47. V. A. Borodin and P. V. Vladimirov, *Diffusion coefficents and thermal stability of small helium-vacancy clusters in iron*, J. Nucl. Mater. **362**, 161 (2007).

48. S. M. H. Haghighat, G. Lucas, and R. Schäublin, *State of pressurized helium bubble in iron*, EPL **85**, 60008 (2009).

49. G. Lucas and R. Schäublin, *Stability of helium bubbles in alpha-iron: A molecular dynamics study*, J. Nucl. Mater. **368-388**, 350 (2009).

50. K. Burke, H. Werschnik, and E. K. U. Gross, J. Chem. Phys. **123**, 062206 (2005).

51. K. Nordlund, 2006, PARCAS computer code. The main principles of the molecular dynamics algorithms are presented in [136, 137]. The adaptive time step and electronic stopping algorithms are the same as in [138].

52. H. J. C. Berendsen, J. P. M. Postma, W. F. Gunsteren, A. D. Nola, and J. R. Haak, *Molecular dynamics with coupling to external bath.*, J. Chem. Phys. **81**, 3684 (1984).

53. G. J. Ackland, M. I. Mendelev, D. J. Srolovitz, S. Han, and A. V. Barashev, *Development of an interatomic potential for phosphorus impurities in alpha-iron*, J. Physics: Condensed Matter **16**, S2629 (2004).

54. P. Olsson, J. Wallenius, C. Domain, K. Nordlund, and L. Malerba, *Two-band modeling of α-prime phase formation in Fe-Cr.*, Phys. Rev. B **72**, 214119 (2005).

55. R. Chakarova, V. Pontikis, and J. Wallenius, Delivery Report WP6, SPIRE project, EC contract no. FIKW-CT-2000-00058 (2002), available at http://www.neutron.kth.se/publications.

56. S. L. Dudarev and P. M. Derlet, *A magnetic interatomic potential for molecular dynamics simulations*, J. Phys.: Condens. Matter **17**, 1 (2005).

57. M. W. Finnis and J. E. Sinclair, *A simple empirical N-body potential for transition metals*, Phil. Mag. A **50**, 45 (1984).

58. D. E. Beck, *A new interatomic potential function for helium*, Mol. Phys. **14**, 311 (1968).

59. G. J. Ackland and R. Thetford, *An improved n-body semi-empirical model for body-centred cubic transition metals*, Phil. Mag. A **56**, 15 (1987).

60. P. M. Derlet, D. Nguyen-Manh, and S. L. Dudarev, *Multiscale modeling of crowdion and vacancy defects in body-centered-cubic transition metals*, Phys. Rev. B **76**, 054107 (2007).

61. C. Björkas, K. Nordlund, and S. Dudarev, *Modelling Radiation Effects Using the Ab-initio Based Tungsten and Vanadium Potentials*, Nucl. Instr. Meth. Phys. Res. B (2008), COSIRES 2008 conference paper, submitted for publication.

62. K. O. E. Henriksson, K. Nordlund, J. Keinonen, D. Sundholm, and M. Patzschke, *Simulations of the initial stages of blistering in helium implanted tungsten*, Physica Scripta **T108**, 95 (2004).

63. W.D. Wilson, R.A. Johnson, in: P.C. Gehlen, J.R. Beeler, R.I. Jaffee (Eds.), Interatomic Potentials and Simulation of Lattice Defects, Plenum, New York, 1972, p. 375.

64. M. S. Daw and M. I. Baskes, *Embedded-atom method: Derivation and application to impurities, surfaces, and other defects in metals*, Phys. Rev. B **29**, 6443 (1984).

65. M. S. Daw, S. M. Foiles, and M. I. Baskes, *The embedded-atom method: a review of theory and applications*, Mat. Sci. Rep. **9**, 251 (1993).

66. C. S. Becquart, C. Domain, A. Legris, and J.-C. van Duysen, *Influence of the interatomic potentials on molecular dynamics simulations of displacement cascades*, J. Nucl. Mater. **280**, 73 (2000).

67. D. Terentyev, C. Lagerstedt, P. Olsson, K. Nordlund, J. Wallenius, and L. Malerba, *Effect of the interatomic potential on the features of displacement cascades in α-Fe: a molecular dynamics study*, J. Nucl. Mater. **351**, 65 (2006).

68. C. Björkas and K. Nordlund, *Comparative study of cascade damage in Fe simulated with recent potentials*, Nucl. Instr. Meth. Phys. Res. B **259**, 853 (2007).

69. D. Terentyev, L. Malerba, R. Chakarova, C. Domain, K. Nordlund, P. Olsson, M. Rieth, and J. Wallenius, *Displacement cascades in Fe-Cr: a molecular dynamics study*, J. Nucl. Mater. **249**, 119 (2006).

70. C. Björkas, K. Nordlund, L. Malerba, D. Terentyev, and P. Olsson, *Simulation of displacement cascades in $Fe_{90}Cr_{10}$ using a two band model potential*, J. Nucl. Mater. **372**, 312 (2008).

71. K. Vörtler, C. Björkas, D. Terentyev, L. Malerba, and K. Nordlund, *The effect of Cr concentration on radiation damage in Fe-Cr alloys*, J. Nucl. Mater. **382**, 24 (2008).

72. K. Vörtler, private communications. To be published.

73. R. Jones and O. Gunnarsson, Rev. Mod. Phys. **61**, 689 (1989).

74. R. M. Martin, *Electronic Structure: Basic Theory and Practical Methods* (Cambridge University Press, Cambridge, Great Britain, 2004).

75. P. Hohenberg and W. Kohn, *Inhomogeneous Electron Gas*, Phys. Rev. **136**, (1964).

76. W. Kohn and L. J. Sham, *Self-Consistent Equations Including Exchange and Correlation Effects*, Phys. Rev. **140**, (1965).

77. J. P. Perdew and A. Zunger, *Self-interaction correction to density-functional approximations for many-electron systems*, Phys. Rev. B **23**, 5048 (1981).

78. J. P. Perdew and Y. Wang, *Accurate and simple analytic representation of the electron-gas correlation energy*, Phys. Rev. B **45**, 13244 (1992).

79. J. A. White and D. M. Bird, *Implementation of gradient-corrected exchange-correlation potentials in Car-Parrinello total-energy calculations*, Phys. Rev. B **50**, 4954 (1994).

80. J. P. Perdew, K. Burke, and M. Ernzerhof, *Generalized Gradient Approximation Made Simple*, Phys. Rev. Lett. **77**, 3865 (1996).

81. P. Träskelin, N. Juslin, P. Erhart, and K. Nordlund, *Hydrogen bombardment simulations of tungsten-carbide surfaces*, Phys. Rev. B **75**, 174113 (2007).

82. P. Träskelin, C. Björkas, N. Juslin, K. Vörtler, and K. Nordlund, *Radiation damage in WC studied with MD simulations*, Nucl. Instr. Meth. Phys. Res. B **257**, 614 (2007).

83. C. Björkas, K. Vörtler, and K. Nordlund, *Major elemental assymetry and recombination effects in irradiated WC*, Phys. Rev. B (Rapid comm.) **74**, 140103 (2006).

84. K. Vörtler and K. Nordlund, *Molecular dynamics simulations of deuterium trapping and re-emission in tungsten-carbide*, J. Phys. Chem. C (2009), invited paper, submitted for publication.

85. K. Inai, Y. Kikuhara, and K. Ohya, *Comparison of carbon deposition on tungsten between molecular dynamics and dynamic Monte Carlo simulation*, Surface and Coatings Technology **202**, 5374 (2008).

86. Z. Insepov, J. Norem, D. Swenson, and A. Hassanein, *Surface erosion and modification by energetic ions*, Vacuum **82**, 872 (2008).

87. Z. Yang, Y. Yang, G.-H. Lu, and G.-N. Luo, *Molecular dynamics simulations of atomic carbon on tungsten surface*, J. Nucl. Mater. **390-391**, 136 (2009).

88. T. Ahlgren, K. Heinola, N. Juslin, and A. Kuronen, *Bond-order potential for point and extended defect simulations in tungsten*, J. Appl. Phys (2009), submitted for publication.

89. C. Björkas, N. Juslin, H. Timko, K. Vörtler, K. Nordlund, K. O. E. Henriksson, and P. Erhart, *Interatomic potentials for the beryllium systems Be, Be-C and Be-H*, J. Phys.: Condens. Matter **21**, (2009).

90. C. Björkas, private communications.

91. X. Wang and L. Andrews, *Neon Matrix Infrared Spectra and DFT Calculations of Tungsten Hydrides WH_x (x=1-4,6)*, J. Phys. Chem. A **106**, 6720 (2002).

92. Gaussian 98 (Revision A.11), M. J. Frisch, G. W. Trucks, H. B. Schlegel, G. E. Scuseria, M. A. Robb, J. R. Cheeseman, V. G. Zakrzewski, J. A. Montgomery, Jr., R. E. Stratmann, J. C. Burant, S. Dapprich, J. M. Millam, A. D. Daniels, K. N. Kudin, M. C. Strain, O. Farkas, J. Tomasi, V. Barone, M. Cossi, R. Cammi, B. Mennucci, C. Pomelli, C. Adamo, S. Clifford, J. Ochterski, G. A. Petersson, P. Y. Ayala, Q. Cui, K. Morokuma, P. Salvador, J. J. Dannenberg, D. K. Malick, A. D. Rabuck, K. Raghavachari, J. B. Foresman, J. Cioslowski, J. V. Ortiz, A. G. Baboul, B. B. Stefanov, G. Liu, A. Liashenko, P. Piskorz, I. Komaromi, R. Gomperts, R. L. Martin, D. J. Fox, T. Keith, M. A. Al-Laham, C. Y. Peng, A. Nanayakkara, M. Challacombe, P. M. W. Gill, B. Johnson, W. Chen, M. W. Wong, J. L. Andres, C. Gonzalez, M. Head-Gordon, E. S. Replogle, and J. A. Pople, Gaussian, Inc., Pittsburgh PA, 2001.

93. A. D. J. Becke, *Density-functional exchange-energy approximation with correct asymptotic behavior*, Phys. Rev. A **38**, 3098 (1988).

94. J. P. Perdew and Y. Wang, *Atoms, molecules, solids, and surfaces: Applications of the generalized gradient approximation for exchange and correlation*, Phys. Rev. B **46**, 6671 (1992).

95. Accelrys Inc., CASTEP Users Guide, San Diego: Accelrys Inc., 2001.

96. V. Milman, B. Winkler, J. A. White, C. J. Pickard, M. C. Payne, E. V. Akhmatskaya, and R. H. Nobes, *Electronic structure, properties, and phase stability of inorganic crystals: A pseudopotential plane-wave study*, Int. J. Quant. Chem. **77**, 895 (2000).

97. DMol is a trademark of AccelRys. Inc.

98. B. Delley, *An all-electron numerical method for solving the local density functional for polyatomic molecules*, J. Chem. Phys. **92**, 508 (1990).

99. *DMol User Guide*, v. 2.3.5 ed., Biosym Technologies Inc., San Diego, California, 1993.

100. L. Laaksonen, P. Pyykkö, and D. Sundholm, *Fully numerical Hartree-Fock methods for molecules*, Computer Physics Reports **4**, 313 (1986).

101. K. Nordlund, N. Runeberg, and D. Sundholm, *Repulsive interatomic potentials calculated using Hartree-Fock and density-functional theory methods*, Nucl. Instr. Meth. Phys. Res. B **132**, 45 (1997).

102. J. F. Ziegler, J. P. Biersack, and U. Littmark, *The Stopping and Range of Ions in Matter* (Pergamon, New York, 1985).

103. J. Moriarty, *Analytic representation of multi-ion interatomic potentials in transition metals*, Phys. Rev. B **42**, 1609 (1990).

104. A. Carlsson, *Angular forces in group-VI transition metals: Application to W(100)*, Phys. Rev. B **44**, 6590 (1991).

105. W. Xu and J. B. Adams, *Fourth moment approximation to tight binding: application to bcc transition metals*, Surface Science **301**, 371 (1994).

106. D. W. Brenner, *Empirical potential for hydrocarbons for use in simulating the chemical vapor deposition of diamond films*, Phys. Rev. B **42**, 9458 (1990).

107. D. W. Brenner, *Erratum: Empirical potential for hydrocarbons for use in simulating the chemical vapor deposition of diamond films*, Phys. Rev. B **46**, 1948 (1992).

108. D. G. Pettifor and I. I. Oleinik, *Analytic bond-order potentials beyond Tersoff-Brenner. I. Theory*, Phys. Rev. B **59**, 8487 (1999).

109. I. I. Oleinik and D. G. Pettifor, *Analytic bond-order potentials beyond Tersoff-Brenner. II. Application to the hydrocarbons*, Phys. Rev. B **59**, 8500 (1999).

110. A. C. T. van Duin, S. Dasgupta, F. Lorant, and W. A. Goddard III, *ReaxFF: A Reactive Force Field for Hydrocarbons*, J. Phys. Chem. A **105**, 9396 (2001).

111. K. Albe, K. Nordlund, and R. S. Averback, *Modeling metal-semiconductor interaction: Analytical bond-order potential for platinum-carbon*, Phys. Rev. B **65**, 195124 (2002).

112. L. Pauling, *The nature of the chemical bond*, 3rd ed. (Cornell University Press, Ithaca, 1960).

113. G. C. Abell, *Empirical chemical pseudopotential theory of molecular and metallic bonding*, Phys. Rev. B **31**, 6184 (1985).

114. J. Tersoff, *New Empirical Model for the Structural Properties of Silicon*, Phys. Rev. Lett. **56**, 632 (1986).

115. J. Tersoff, *New empirical approach for the structure and energy of covalent systems*, Phys. Rev. B **37**, 6991 (1988).

116. K. Albe, *Computersimulationen zu Struktur und Wachstum von Bornitrid*, Ph.D. thesis, Technische Universitat Dresden, 1998.

117. K. Albe, K. Nordlund, J. Nord, and A. Kuronen, *Modeling of compound semiconductors: Analytical bond-order potential for Ga, As, and GaAs*, Phys. Rev. B **66**, 035205 (2002).

118. J. Nord, K. Albe, P. Erhart, and K. Nordlund, *Modelling of compound semiconductors: Analytical bond-order potential for gallium, nitrogen and gallium nitride*, Journal of Physics: Condensed Matter **15**, 5649 (2003).

119. W.D. Wilson, Conference on Fundamental Aspects of Radiation Damage in Metals, USERDA-CONF-751006-P2, vol. 1025, 1975.

120. T. Seletskaia, Y. Osetsky, R. E. Stoller, and G. M. Stocks, *Magnetic Interactions Influence the Properties of Helium Defects in Iron*, Phys. Rev. Lett. **94**, 046403 (2005).

121. T. Seletskaia, Y. N. Osetsky, R. E. Stoller, and G. M. Stocks, *Calculation of helium defect clustering properties in iron using a multi-scale approach*, J. Nucl. mater. **351**, 109 (2006).

122. T. Seletskaia, Y. N. Osetsky, R. E. Stoller, and G. M. Stocks, *Development of a Fe-He interatomic potential based on electronic structure calculations*, J. Nucl. mater. **367-370**, 355 (2007).

123. G. Kresse *et al.*, *Ab initio molecular dynamics for liquid metals.*, Phys. Rev. B **47**, 558 (1993), *ibid.*, Phys. Rev. B, 49 (1994) 14251; Comput. Mat. Sci., 6 (1996) 15; Phys. Rev. B, 54 (1996) 11169.

124. R. Hafner, D. Spisak, R. Lorenz, and J. Hafner, *Does density-functional theory predict a spin-density-wave ground state for Cr?*, J. Phys.: Condens. Matter **13**, L239 (2001).

125. R. Hafner, D. Spisak, R. Lorenz, and J. Hafner, *Magnetic ground state of Cr in density-functional theory*, Phys. Rev. B **65**, 184432 (2002).

126. D. A. Terentyev, L. Malerba, and M. Hou, *Dimensionality of interstitial cluster motion in bcc-Fe*, Phys. Rev. B **75**, 104108 (2007).

127. K. Nordlund, J. Wallenius, and L. Malerba, *Molecular dynamics simulations of threshold energies in Fe*, Nucl. Instr. Meth. Phys. Res. B **246**, 322 (2005).

128. P. G. Lucasson and R. M. Walker, *Production and Recovery of Electron-Induced Radiation Damage in a Number of Metals*, Phys. Rev. **127**, 485 (1962).

129. J. N. Lomer and M. Pepper, *Anisotropy of defect production in electron irradiated iron*, Phil. Mag. **16**, 119 (1967).

130. F. Maury, M. Biget, P. Vajda, A. Lucasson, and P. Lucasson, *Anisotropy of defect creation in electron-irradiated iron crystals*, Phys. Rev. B **14**, 5303 (1976).

131. C. Björkas and K. Nordlund, *Assessment of the relation between ion beam mixing, electron-phonon coupling, and damage production in Fe*, Nucl. Instr. Meth. Phys. Res. B (2009), accepted for publication.

132. L. Yang, X. T. Zu, H. Y. Xiao, F. Gao, K. Z. Liu, H. L. Heinisch, R. J. Kurtz, and S. Z. Yang, *Temperature effects on He bubbles production due to cascades in α-iron*, Mater. Sci. Eng. A **427**, 343 (2006).

133. L. Yang, X. T. Zu, H. Y. Xiao, F. Gao, H. L. Heinisch, R. J. Kurtz, and K. Z. Liu, *Atomistic simulation of helium-defect interaction in alpha-iron*, Appl. Phys. Lett. **88**, 091915 (2006).

134. J. Yu, G. Yu, Z. Yao, and R. Schäublin, *Synergistic effects of PKA and helium on primary damage formation in Fe-0.1%He*, J. Nucl. Mater **367-370**, 462 (2007).

135. G. Lucas and R. Schäublin, *Helium effects on displacement cascades in α-iron*, J. Phys.: Condensed Matter **20**, 415206 (2008).

136. K. Nordlund, M. Ghaly, R. S. Averback, M. Caturla, T. Diaz de la Rubia, and J. Tarus, *Defect production in collision cascades in elemental semiconductors and FCC metals*, Phys. Rev. B **57**, 7556 (1998).

137. M. Ghaly, K. Nordlund, and R. S. Averback, *Molecular dynamics investigations of surface damage produced by keV self-bombardment of solids*, Phil. Mag. A **79**, 795 (1999).

138. K. Nordlund, *Molecular dynamics simulation of ion ranges in the 1 – 100 keV energy range*, Comput. Mater. Sci. **3**, 448 (1995).